AFIT/GAP/ENP/95D-2

MICROMIRROR ARRAY CONTROL OF A PHASE-LOCKED LASER DIODE ARRAY

THESIS

Carl J. Christensen, Captain, USAF

AFIT/GAP/ENP/95D-2

Approved for public release; distribution unlimited.

AFIT/GAP/ENP/95D-2

MICROMIRROR ARRAY CONTROL OF A PHASE-LOCKED LASER DIODE ARRAY

Carl J. Christensen, B. A.
Captain, USAF

Approved: Date

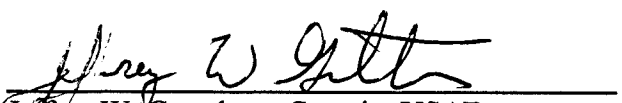

Jeffrey W. Grantham, Captain, USAF
Chairman, Thesis Committee

20 Nov 95

Dr. Won B. Roh
Member, Thesis Committee

27 Nov 95

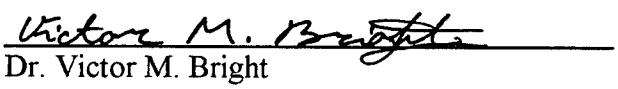

Dr. Victor M. Bright
Member, Thesis Committee

30 Nov 95

AFIT/GAP/ENP/95D-2

MICROMIRROR ARRAY CONTROL OF A PHASE-LOCKED LASER DIODE ARRAY

THESIS

Presented to the Faculty of the Graduate School of Engineering

of the Air Force Institute of Technology, Air University

in Partial Fulfillment of the

Requirements for the Degree of

Master of Science in Engineering Physics

Carl J. Christensen, B. A.

Captain, USAF

December 1995

Acknowledgments

This work would not have been possible without the assistance provided by many people. I am grateful to Dr. Won Roh for providing the lasers used for these experiments. I would like to thank Dr. Victor Bright for bringing the Micro Electrical Mechanical Systems technology to the attention of the Physics Department, and Major John Comtois for designing the micromirror array. I am especially indebted to Captain Jeffrey Grantham. He developed the original premise for this research and provided the support and advice necessary to keep the research effort on track.

Finally, I would like to express my gratitude to my wife, Donna, and my daughters, Sarah and Kelly. They provided the continuous support and encouragement that kept me going over the past 18 months. There were times when it must have seemed like the lab and my computer were more important to me than them. Nothing could be further from the truth, and their understanding during those difficult times is appreciated.

Carl J. Christensen

TABLE OF CONTENTS

LIST OF FIGURES

LIST OF TABLES

Abstract

A ten element micromirror array has been designed, fabricated, and employed to control the far-field irradiance pattern of a phase-locked laser diode array. The laser array used in this experiment was a ten element, gain guided array lasing at a nominal wavelength of 828 nm and operating in the π out-of-phase supermode. The laser's near-field irradiance was imaged onto a micromirror array, where the π phase differences between adjacent laser elements were corrected. This was accomplished by moving the micromirrors with individually applied voltages. The result was the desirable single lobed far-field pattern, placing the maximum amount of laser power on a single spot.

The micromirror array was also used to phase steer the reflected laser beam. In analogy to phased array radar steering, a small phase difference was introduced between adjacent elements of the array. The phase front introduced across the array steered the single lobe, resulting in beam deflections from -0.480° to +0.327° from the normal to the array.

MICROMIRROR ARRAY CONTROL OF A PHASE-LOCKED LASER DIODE ARRAY

I. Introduction

Laser Applications

Since the first laser was demonstrated in 1960, myriad uses for lasers in support of the United States Air Force (USAF) mission "to defend the United States through control and exploitation of air and space" have been found. Lasers are currently utilized for tasks such as: range finding, target designation, weapon guidance, communications, infrared (IR) aiming, and weapons simulation. Research and development is ongoing in many other applications, including: chemical warfare agent detection, laser radar, laser blinders, space communications, directed energy weapons, electro-optic countermeasures, and energy transport.[1,2]

The advances made in laser technology research for military applications also benefit the civilian community. Commercial applications of lasers include: laser printers, optical recording, barcode scanners, fiber-optic transmission, compact disc players, pumping of other lasers, and medical applications.

Semiconductor Lasers

There is a class of lasers that is perfectly suited for many of these applications. Semiconductor lasers, also referred to as laser diodes (LDs), have matured to the point where they are practical for everyday use. The development of double heterostructures in the 1970's made continuous operation at room temperature possible.[3] Military and civilian applications can greatly benefit from the use of these durable, compact devices. Their advantages include small size, light-weight, low cost, long lifetimes, and high efficiency. A typical laser diode and its dimensions are shown in Figure 1a.

The drawback to semiconductor lasers is that their maximum output power is limited. Optical power density at the laser diode emitter is limited due to the small size of the emitter. High currents at the emitter will lead to facet damage, and emitters with larger active regions also tend to fail prematurely. Therefore, for high power, laser diodes are packaged into arrays. Multiple coherently coupled small emitters in a multi-stripe array offer a simple, practical way to get high total power.[4] A typical laser diode array (LDA) is shown in Figure 1b.

LDAs can operate either coherently or incoherently. If coupling between elements does not occur the array operates incoherently. But if the elements of the array are spaced closely enough together, the evanescent electric field waves of the element will couple with those of other elements in the array. The strongest phase coupling occurs with an element's nearest neighbors. This optical coupling locks the phase between adjacent beams and the array operates coherently. Many phase-locked modes, also called supermodes are possible, an N element array can operate in N different supermodes.[5]

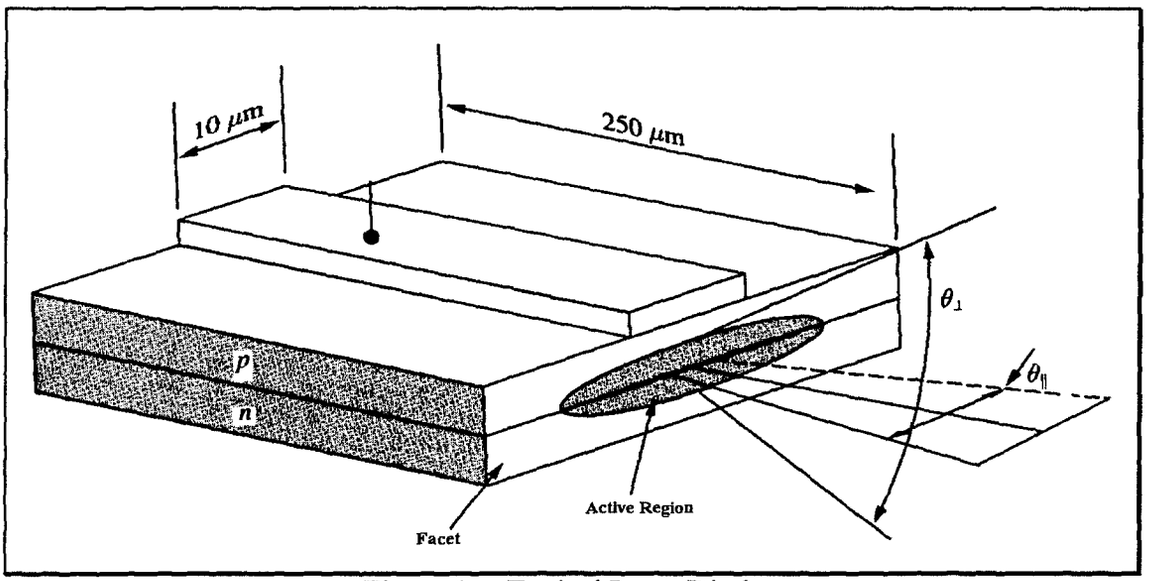

Figure 1a. Typical Laser Diode.

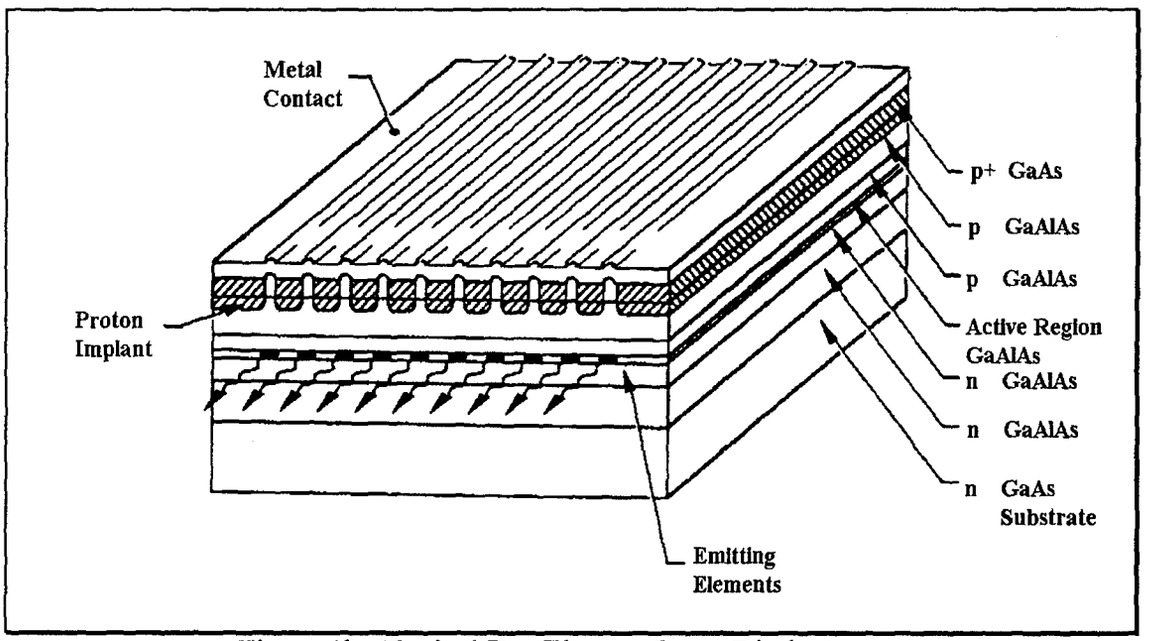

Figure 1b. Typical Ten Element Laser Diode Array.

Of these possible supermodes, two are of special interest. In the lowest order supermode (n=1) the individual elements operate with a 0° phase difference ($\Delta\phi$) between them. This leads to a single lobed far-field intensity pattern. On the other hand, if the laser operates in the highest order supermode (n=N), $\Delta\phi$ will be 180° and the far-field intensity pattern will have two lobes.

The phase relationship between elements is not always controllable. The phases adjust themselves to minimize laser threshold current (I_{TH}). Since the gain is reduced in the region between elements, the field tends to be a minimum there.[5] If $\Delta\phi$ is 180° the electric field across the array passes through zero at a point midway between the elements and therefore this mode is favored. This supermode is also favored at higher currents because it has a higher net gain. Therefore, LDAs with uniform elements tend to operate in a stable 180° mode[6] and thus they will produce a two lobed far-field pattern. To make matters worse, many LDAs will change modes as the input current is increased.

Recently, resonant antiguided arrays have been developed. These arrays operate in the in-phase mode.[7] Unfortunately, antiguided LDAs are still in the research stage and not yet commercially available.

In general then, it is seen that by packaging laser diodes into arrays high powers are attainable, but usually at the expense of a diffraction limited single lobe intensity pattern. Thus, there is clearly a need for a method of correcting and controlling the phasing of laser diode arrays.

Statement of the Problem

For most laser applications, it is desirable to have the maximum output power of the laser concentrated into a single lobed, diffraction limited, far-field pattern. Typical laser diode arrays have a dual lobed irradiance pattern in the far-field. Therefore, the two goals of this project will be to investigate and demonstrate new techniques to:

A. Produce a single lobed far-field intensity pattern from a LDA operating in the highest order supermode ($\Delta\phi = 180°$).

B. Steer the single lobe in the far-field.

These objectives are attainable by altering the phasing of the individual elements of the LDA in the near-field. The relative phases of the elements can all be set in-phase, leading to a single lobed far-field intensity pattern, using a micromirror array. The near-field of the LDA will be imaged onto the micromirror array using a 10 × objective lens. Adjustments of the mirrors will be made to change the optical path length difference between elements, thereby altering the phase difference between the LDA elements. Since the mirror deflections are adjustable, any desired phase front can be created across the micromirror array. Alignment of the mirrors will then be made to phase steer the single lobe in the far-field. Experiments will be performed to characterize the operating parameters and intensity patterns of the LDA with and without the mirrors in place.

Approach and Presentation

The fundamental theory of LDAs will be presented as a foundation. Previous efforts to produce a single lobed pattern in the far-field, and previous steering techniques will be discussed. The theory for the micromirror array and how the device was built will also be presented.

The experimental portion of this investigation will consist of four phases. First, the LDA will be characterized in terms of: average output power, threshold current, emission spectra, separation between lobes, and near and far-field intensity patterns. The phase difference between adjacent elements of the LDA will be measured. Next, the micromirror array will be characterized. The key measurement to be made will be mirror deflection versus voltage. The amount of laser power reflected by the mirrors into the far-field pattern will also be measured. A single lobe in the far-field will be demonstrated and optimized by using the micromirror array to set $\Delta\phi = 0°$ between LDA elements. Finally, the micromirror array will be used to alter the phase front across the LDA and steer the laser beam.

II. Background

Semiconductor Laser Theory

If a positive voltage is applied to the p side of a p-n junction, and a negative voltage to the n side, the junction is said to be forward biased. When a semiconductor laser is forward biased, the applied voltage causes holes and electrons to be injected into the active layer of the laser diode (LD). Recombination of holes and electrons causes photons to be emitted. Some of these photons are reflected at the end facets of the semiconductor. Spontaneously emitted photons and the reflected photons will cause stimulated emission of more photons as they travel down the length of the semiconductor, quickly escalating the number of photons in the cavity. When the photon gain surpasses photon loss, lasing occurs. The photons that are transmitted through the end facets emerge as narrow band coherent light.

The semiconductor laser diode or LD was invented in 1962. The first LDs were made of GaAs doped to form a p-n junction. These lasers were called homostructures, because they were made of only a single material. They had a very high lasing threshold current (I_{TH}) and so could only be operated in pulsed mode and at cryogenic temperatures. The tremendous heat created by these early small devices would cause them to overheat and fail if operated in continuous wave (CW) mode.[8]

Laser Construction

It is possible to lower the I_{TH} of a LD through the use of double heterostructures. A heterostructure is a combination of two dissimilar materials. The double heterostructure is formed by sandwiching a direct bandgap material (i.e. GaAs) between two layers of semiconductor material with a higher bandgap. The most common type of these devices uses GaAs and $Al_xGa_{1-x}As$ where x is the fraction of Ga replaced by Al. Holes and electrons from the $Al_xGa_{1-x}As$ layers injected into the GaAs layer will become trapped in a potential well formed by the $Al_xGa_{1-x}As$ /GaAs/$Al_xGa_{1-x}As$ layers. Figure 2 illustrates the band gap and refractive index differences between GaAs and $Al_xGa_{1-x}As$. This phenomenon is called carrier confinement and causes many holes and electrons to be packed into a small volume. The $Al_xGa_{1-x}As$ not only has a higher bandgap than GaAs, it also has a lower index of refraction. Regions of lower refractive index material flanking the active region act as an optical waveguide, confining photons in the active region. These effects combine to yield more gain, higher efficiency and a lower I_{TH}.[9]

Common LDs are constructed by epitaxially growing AlGaAs layers on a GaAs substrate. The GaAs layer forms the active layer, so the width of the active region is defined by the width of this layer. After the semiconductor crystal is grown, the crystal is cleaved perpendicular to the plane of the p-n junction, creating a partially reflecting facet at the ends of the crystal. The refractive index of the semiconductor materials used to build lasers is approximately 3.6, leading to about 30% reflection of photons at the air/ semiconductor interface. Due to the high gain of the device caused by carrier confinement, this low reflection is enough to initiate lasing.[5]

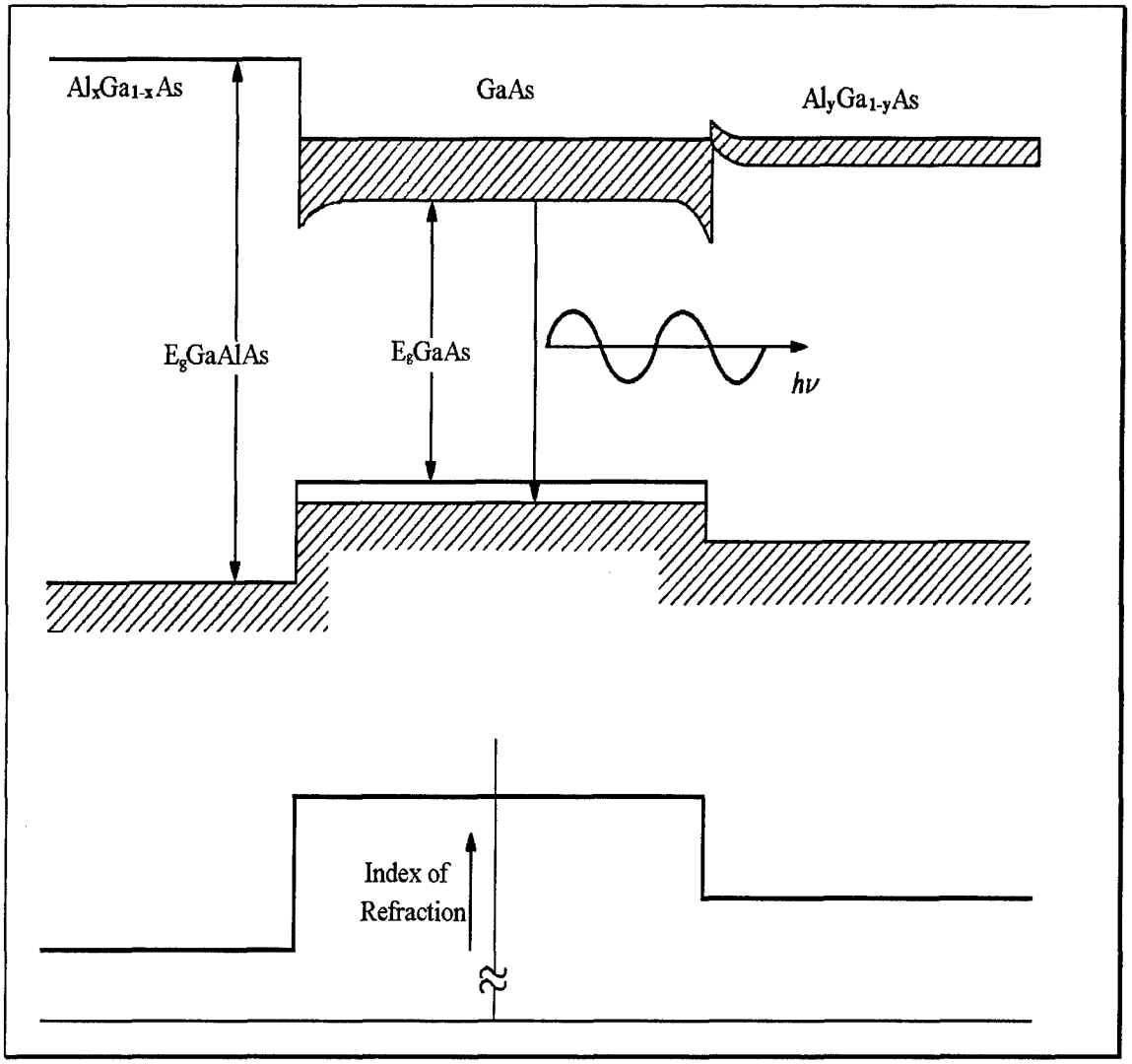

Figure 2. Band Gap and Index of Refraction of Double Heterostructures.

Stripe Geometry

The width of the active region in a LD can be narrowed in two dimensions instead of just one. This method of confining the gain region is called stripe-geometry. Stripe-geometry LDs can be broken into classes, index-guided, gain-guided, and antiguided.

Index-guided LDs use a physical waveguide structure to confine the laser light to the active region. The narrow active region is surrounded on four sides by materials with lower indices of refraction than that of the active region. This optical confinement traps both the light and the charge carriers. Index-guided structures can have very small active regions $\approx 1\mu m$ and therefore are very efficient.[3]

Gain-guided LDs also use index-guiding, but only in the plane perpendicular to the p-n junction. In the parallel plane, a layer of insulating material with a thin strip of exposed metal is placed between the positive contact and the rest of the structure. This thin strip carries current into the active region and establishes the gain region. Since there is no structure confining the beam in the parallel plane, gain-guided lasers tend to have a broader less coherent light beam. But this larger active area also allows them to reach higher powers than index-guided lasers.[3,10]

Antiguided LDs can be either gain-guided or index-guided in construction, but they also have a unique additional feature; a lower effective index of refraction in the center of the active region. This low index region causes divergence of the radiation, and in turn the field strength is then stronger at the edges of the emitter, leading to stronger coupling between elements. Antiguided arrays can be physically constructed by using a highly

refractive material for the interelement region or antiguiding can be caused by a high electron concentration in the center of the active region. Antiguded arrays operate in "leaky array modes". They favor only the in-phase or out-of-phase supermodes due to their strong interelement coupling. The lasing mode depends upon the specific structure under consideration.[7,11]

Previous Work: Single Spot in the Far-Field

In the quest for higher power from LDs, two avenues have been explored. Early research centered around increasing the size of the active region. Unfortunately, it is not possible to achieve stable high power operation of a LD as the size of the element is increased. Large regions generate uncontrollable transverse modes and filamentary oscillation that will destroy the device. It was discovered that to achieve high powers, LDs should be packaged into arrays. As mentioned earlier, a multi-stripe array of emitters offers a practical way to get high total power. In 1978, Scifres *et al.* reported the first LDA, a five element gain-guided device.[7] This device and gain-guided arrays in general operate in out-of-phase supermodes with multiple lobes in the far-field. In order to fully exploit this source of optical energy, the maximum output power must be concentrated in a single diffraction limited lobe in the far-field:

$$\text{Diffraction Limit} = \frac{\lambda}{NS} \text{ (radians)} \qquad (2.1)$$

where λ is the wavelenth, N is the number of elements in the array, and S is the center-center spacing of the elements. Many researchers have proposed and demonstrated

procedures to obtain a single lobe intensity pattern in the far-field of a LDA. In general, two approaches have been used; combining the far-field lobes into a single spot, or altering the phasing in the near-field.

A diffraction limited circular spot was obtained by Tatsuno *et al.* using anamorphic prism optics to combine lobes in the far-field. This method also required the aid of a polarization beam combiner and a phase shifter.[12] Summers studied the effects of using glass cubes as an optical delay line and employing a $\lambda/2$ waveplate to combine two lobes in the far-field into one. He was able to obtain a non-diffraction limited single lobe containing up to 84% of the total laser power.[10]

Several types of external cavities have been used to alter the intensity pattern of LDAs. One example of this is a Talbot cavity. The Talbot effect is a diffraction phenomenon where exact images of an infinite periodic object are formed at certain distances from the object plane.[13] Waarts *et al.* used an external Talbot cavity to coherently combine the outputs of a LDA in the far-field. A semireflecting output mirror placed a Talbot distance from a 20 element array was used to coherently combine their outputs. The far-field intensity pattern they produced remained diffraction limited at powers up to 250 mW CW. Leger, Scott, and Veldkamp utilized a microlens array and a feedback mirror in a Talbot cavity. The lenses collimated the beams and diffractive coupling in the cavity provided coherent coupling of the output. A single lobed far-field pattern was produced, with 82% of the array's output power in the central lobe.[14]

Chang-Hasnain *et al.* also utilized an external cavity to obtain a single lobe in the far-field. A graded refractive index (GRIN) lens imaged the near field of a LDA onto an

apertured mirror. The mirror provided selective feedback for the fundamental supermode (n=1). With the array thus phase-locked, 94% of array's total output power was contained in an "extremely clean single-lobed far field" pattern.[15] Segev and Fischer built an external cavity with a slit and phase conjugate mirror. The slit acted as a filter that favored the lowest order supermode. The effect of slit width was analyzed, and it was found that different slit widths would favor different supermodes.[16] Jackson *et al.* constructed an external cavity consisting of a collimating lens and a diffraction grating. Control of the grating angle allowed selection of the LDA supermode. But as the input current was increased beyond $1.3 \times I_{TH}$, the out-of-phase supermode dominated the output.[17]

An interesting study was performed by Beernik *et al.* using InGaAs strained layer active regions in GaAs-AlGaAs semiconductors. The analysis of these gain-guided arrays predicted in-phase operation of the LDA when the elements were less than some critical spacing apart. This is due to the antiguiding of the InGaAs layers. Five stripe arrays were grown with interelement spacings of 14, 15, and 30 μm. The LDA with 30 μm spacing operated with a 180° phase difference between adjacent elements, and a two lobed far-field pattern. The arrays with 14 and 15 μm spacing operated with the emitters in-phase. These LDAs maintained in-phase operation at injection currents up to $3\ I_{TH}$, exhibiting the desirable narrow single lobe in the far-field.[18]

Injection locking studies have shown promise as well, though the need for an external master oscillator makes the method somewhat cumbersome. Hohimer *et al.* reported a single far-field lobe by optical injection of a single frequency laser into one end element

of a LDA. However, the far-field beam angle increased with increased injection frequency.[19] Hohimer also participated in a study of the possibilities of using this change in the far-field beam angle to scan the beam.[20] Chun *et al.* developed a numerical model for injection locking. They noted that injection of a master oscillator into any element of a LDA would result in a single spectral mode output, but only injection at one of the end elements will result in in-phase operation producing a single lobe in the far-field.[21]

Self-injection, using a phase-conjugate mirror to reflect the array output back into the stripes has been attempted. MacCormack and Eason performed experiments where self-injection phase-locked the array in the lowest order supermode. Single lobe outputs were obtained, their width was 2.2 × the diffraction limit, and up to 75% of the total power was contained in the output. Unfortunately, they were unable to self-start the feedback without using an external locking laser to control the initial output from the array.[22]

Phase shifting individual elements of a LDA in the near-field offers an elegant, compact means of obtaining a single lobe intensity pattern in the far-field. Several groups have demonstrated in-phase operation using phase shifters.

Taneya *et al.* fabricated a phase shifter by depositing SiO_2 and Si_3N_4 layers on a glass substrate. The amount of phase shift was determined by the thickness of the Si_3N_4 layer, which was etched to provide a 150° phase shift to every other element. The phase shifter was aligned with the elements of the LDA and a stable single lobe was observed in the far-field. There were some side lobes present since the phase shift was not quite 180°. Power up to 200 mW was obtained.[23] Expanding on this work, Matsumoto, Taneya *et al.* demonstrated an integrated phase shifter. Al_2O_3 film was applied directly to the front

facet of an array, the film thickness was varied to give a 180° phase shift at every other element. A single lobed far-field pattern was obtained, the full width at half maximum (FWHM) of the output was 3.3° at 2.1 I_{TH}, which was 1.1 × the diffraction limit. At higher currents broadening occured due to the prescence of other array modes.[24]

Thaniyavarn and Dougherty used a variable phase shift zone plate mounted next to the laser output facet to obtain a single far-field lobe. Variable thickness dielectric film strips were deposited on a microslide, the width and spacing of the strips were chosen to align the strips with every other element of the LDA. A Spectra Diode Labratories ten element phase locked diode array operating in a stable out-of-phase mode was used. The zone plate was epoxied in front of the output facet once the proper relative positioning was achieved. The far-field pattern exhibited a single narrow lobe in accord with their expectations.[25]

Previous Work: Steering of a Beam

The steering of a collimated laser beam is a fundamental building block for many optical systems such as laser radar, barcode scanners, and laser printers. Traditionally, this function has been performed by mirrors. But bulk optical components such as mirrors are too heavy for rapid optical beam scanning. Therefore, other methods for beam steering have been studied. Rapid beam steering capability in a small lightweight package has been obtained by many groups with varying success.

One method that has received much attention employs binary optics microlens arrays and Galilean telescope geometry. Binary optics use high resolution lithography and ion beam etching to transfer binary or multi-step relief patterns onto dielectric or metallic substrates. The lens functions as a Fresnel phase zone pattern where circular gratings diffract light to a common focus. Galilean telescope geometry predicts that a plane wave incident on the optic axis of an afocal lens system will exit tilted with respect to the axis if the lenses are not laterally centered. Therefore, translation of one lens with respect to the other will steer the beam.[26]

Goltsos and Holz used the above described method to achieve steering over an 11° field of view. A collimated He-Ne laser beam was used to illuminate an array of 200 μm diameter lenses. A second array, 10 μm from the first, was laterally displaced to steer the beam. The beam could be steered at a 35 Hz rate. Predicted efficiency was 95%, but only 59% efficiency was achieved. The difference was attributed to deficiencies in the manufacture of the lenses.[26]

Motamedi *et al.* also fabricated arrays of lenses to steer a beam. Their array was 10 × 10 mm, each square lens was 200 μm on a side. Piezoelectric transducers were used to translate one of the arrays in two dimensions. 25 μm of array translation produced 2.5° of steering. A 300 Hz steering rate and 50% efficiency was reported.[27]

Farn employed phased arrary like binary optics in a similar fashion. Instead of lenses, his optical elements were phase plates. The second plate produced a variable phase change as it was moved in the plane parallel to the first. The design was intended to yield a 6° FOV in two dimensions with 120 μm of plate translation. In Farn's validation he

compared his design to a lens array and averaged 20% higher efficiency, with less than 1% intensity in the first order sidelobe.[28]

Sun *et al.* steered a semiconductor laser by arranging the elements of the array in a fan-like fashion. The elements were aligned so that they all focused on a common front mirror. By individually addressing the elements a number of fixed angles could be obtained. With 11 elements in the device, a total scan of 80° in ≈ 7° steps was reported.[29]

Liquid crystal devices are another realm being explored for their beam steering possibilities. Kenyon studied the properties of a liquid crystal display from a commercial pocket television and found that it could not produce enough phase shift (180°) to produce a single lobe in the far-field,[30] but the phase shifting abilities of a LCD can be used to steer a beam.

Zhou, Yeh, and Liu utilized a liquid crstal television display as an electronically addressed spatial light modulator (ESLM). The ESLM simulates a computer generated hologram which in turn reconstructs a beam pattern stored in a photorefractive crystal. Two dimensional steering up to 20° and a theoretical efficiency of 46% was noted.[31]

Wright Laboratories has studied liquid crystals as well. In their work, McManamon and Watson are developing writable liquid crystals in a phased array for use in laser radars. The theory is the same as that employed in microwave phased array radars. They have demonstrated one dimensional steering of 0.53, 1.06, and 10.6 μm wavelength lasers. The 1.06 μm laser has been steered to 0.24° with 97% efficiency, 1.9° with 85% efficiency, and 3.8° with 57% efficiency. Sidelobe supression was not addressed in their studies.[32]

III. Theory

In this work, the micromirror array is employed as a phase shifter to create a single lobed intensity pattern from a laser diode array (LDA) and also to phase steer the single lobe. This method has distinct advantages over the methods discussed in the previous chapter. The phase shifters described in Chapter II were limited to a fixed amount of phase shift dictated by their thickness. The micromirror array is not bound by such a limitation. The micromirror array can apply any amount of phase shift from 0 to 2 π radians by deflection of the mirrors, and each mirror can be moved independently. Therefore, the micromirror array can apply any desired phasing to the output of the LDA. This unique feature enables creation of a single lobed far-field intensity pattern and phase steering of the laser output from a single device.

The Micromirror Array

The micromirror array adjusts the phasing of the LDA by introducing an optical path difference (OPD) between elements before they are combined in the far-field. To accomplish this, the mirrors are deflected from their rest position by applying a D. C. voltage to their address electrodes. The mirrors are independently addressable, so each one can be positioned separately, consequently any phase difference ($\Delta\phi$) can be set up between the elements of the LDA.

A small hole (~ 5 μm diameter) was left in each mirror to facilitate etching of the photosilicate glass beneath them during manufacture. Appendix A describes the array and the manufacturing process. The hole will be exploited to determine mirror deflection versus applied voltage.

If a HeNe laser beam ($\lambda = 632.8$ nm) is focused onto a single mirror in the array so that it strikes the mirror and the etch hole simultaneously, light will be reflected from both the mirror and the address electrode beneath it. Since the light is coherent, an interference pattern will result when the reflected light is observed on a screen. The irradiance at the center of the interference pattern is given by:

$$I = I_1 + I_2 + 2\sqrt{I_1 I_2} \cdot \cos\Delta\phi \tag{3.1}$$

where I_1 is the intensity of light reflected from the mirror, I_2 is the intensity of light reflected from the address electrode, and $\Delta\phi$ is the phase difference between the two. As the mirror moves up or down in relation to the address electrode, $\Delta\phi$ between the two reflected sources will change. As a result, the center of the interference pattern will go from bright to dark to bright again repeatedly as the mirror moves. Maximum intensity occurs when $\Delta\phi = \pm 2m\pi$, where m is an integer. Minimum intensity occurs when $\Delta\phi = \pm(2m + 1)\pi$. Therefore:

$$I_{MAX} = I_1 + I_2 + 2\sqrt{I_1 I_2} \tag{3.2}$$

and

$$I_{MIN} = I_1 + I_2 - 2\sqrt{I_1 I_2} \tag{3.3}$$

Equations 3.1 - 3 give three equations in three unknown quantities; I_1, I_2, and $\Delta\phi$. Algebraic manipulation yields:

$$I = \frac{I_{MAX} + I_{MIN}}{2} + \frac{1}{2}\left(I_{MAX} - I_{MIN}\right)\cdot\cos(\Delta\phi) \tag{3.4}$$

and

$$\Delta\phi = \cos^{-1}\left[\frac{2I - (I_{MAX} + I_{MIN})}{I_{MAX} - I_{MIN}}\right] \tag{3.5}$$

Mirror deflection can be calculated by measuring the change in intensity at the center of the interference pattern. Intensity as a function of voltage is recorded as the voltage to the mirror is varied. Figure 3a illustrates a typical intensity-voltage curve.

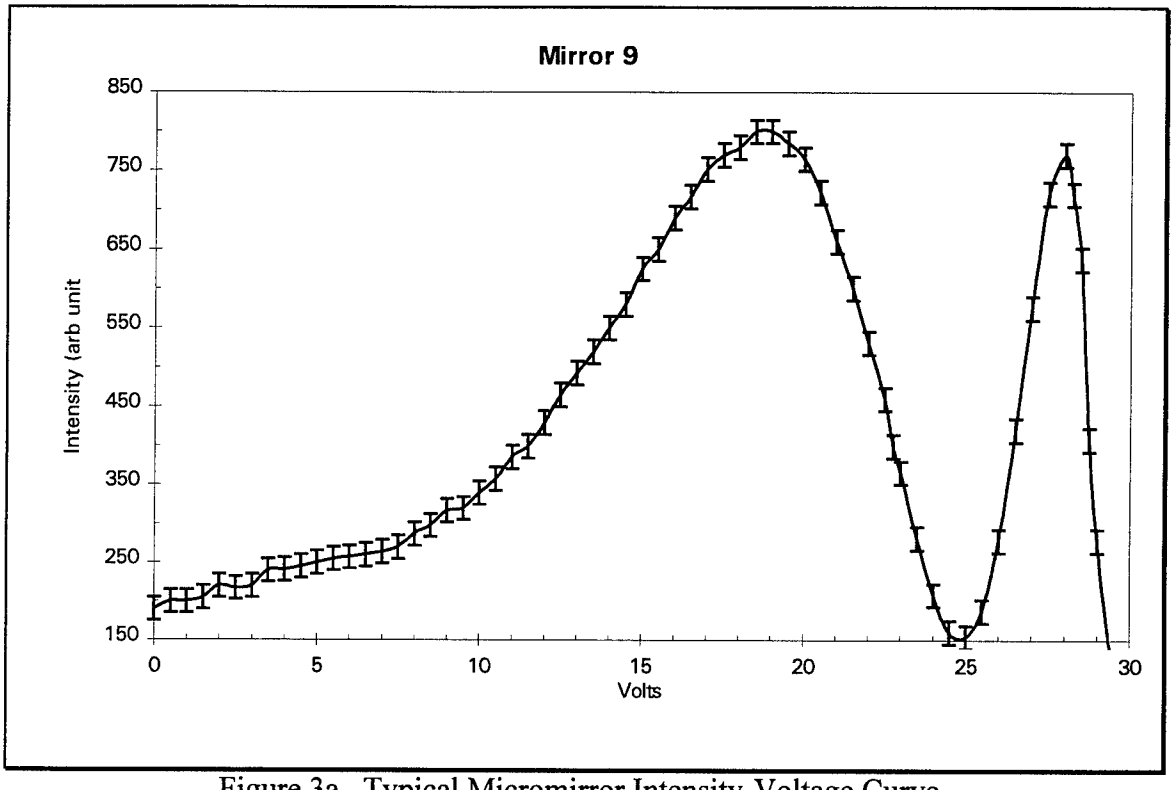

Figure 3a. Typical Micromirror Intensity-Voltage Curve.

From the intensity plot, maxima (I_{MAX}) and minima (I_{MIN}) are noted. If I_{MAX} and I_{MIN} are known, $\Delta\phi$ can be calculated for any applied voltage[8] using Equation 3.5. Mirror deflection (d) is related to phase by :

$$d = \frac{(\Delta\phi)\cdot\lambda}{4\pi} \tag{3.6}$$

Figure 3b shows the results for mirror 9 of the micromirror array used.

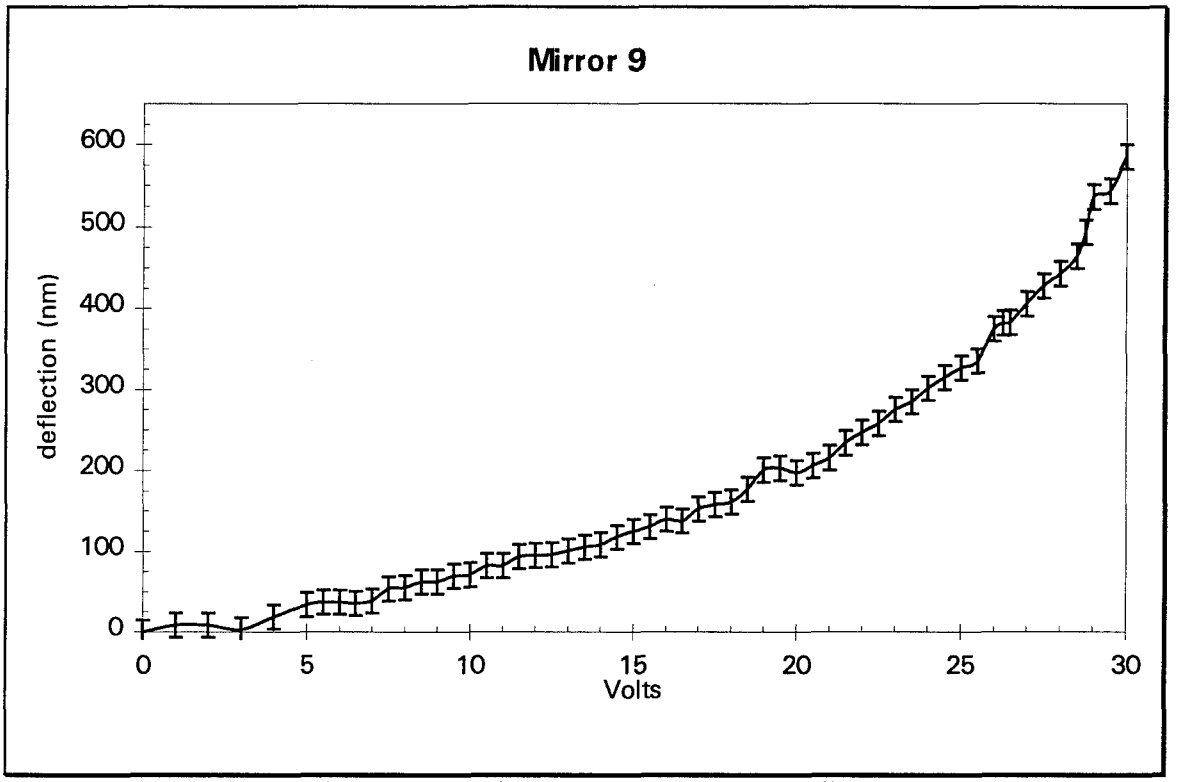

Figure 3b. Mirror Deflection Curve Corresponding to the Intensity-Voltage Curve in Figure 3a.

Laser Diode Array Modes

Coupling between electric fields of adjacent elements in a LDA causes the array to operate in phase-locked modes. Two different theories have been used to determine the far-field intensity pattern from a phase-locked LDA. Coupled mode theory was first published by Butler *et al.*[33] According to Botez, experiments by Paoli *et al.* and Epler *et al.* confirmed that coupled mode analysis best describes phased-locked array behavior. Coupled mode theory shows that an N element array can operate in N eigenmodes[34], also

called supermodes. From this theory the near-field electric field distribution is given by Segev and Fischer as:

$$E_v(y) = \sum_{l=1}^{N} \sin\left(\frac{\pi \cdot mv}{N+1}\right) \cdot \exp\left[-\frac{(y_o - nD)^2}{2\sigma^2}\right] \tag{3.7}$$

where υ is the array supermode, m is the element number, N is the total number of elements, $n = 2 \cdot m - (N+1)$ gives the displacement from the end of the array to the element, 2D is the spacing between elements, and σ is the Gaussian width of the elements.[16]

On the other hand, simple diffraction theory can also be used to analyze the behavior of phase-locked arrays. Scifres *et al.* were the first to analyze phase-locked LDAs using simple diffraction theory. This theory accurately predicts the patterns for supermodes where $\Delta\phi$ between adjacent elements is constant. Thus, it can be used for the two simplest LDA supermodes; the in-phase ($\Delta\phi = 0°$) supermode and the out-of-phase ($\Delta\phi = 180°$) supermode. As was mentioned in the introduction, these two modes are of special interest; the in-phase supermode because it concentrates the most laser power in a single diffraction limited spot, and the out-of-phase supermode because many commonly available LDAs operate in this mode.

The electric field of the LDA at the emitting facet can be modeled as a rectified cosine function. Inside the waveguides of the array the electric field is a cosine, and outside the waveguide in the region between elements it is a rapidly decaying exponential function.[35] It is these decaying (evanescent) waves that lead to interaction and phase-locking, but the decaying portion dies off quickly enough that it can be ignored for

calculation of the far-field intensity pattern. Therefore, we can approximate the near-field electric field distribution of the LDA at the emitting facet as:

$$E_{NF}(x) = E(0) \cdot \sum_{n=1}^{N} \cos\left(2\pi \frac{(x-nb)}{2b}\right) \cdot rect\left(\frac{x-nb}{b}\right) \cdot \exp(in\Delta\phi) \qquad (3.8)$$

In this expression, n = 1, ..., N are the individual elements, x is the distance from the end of the array to the nth element, b is the spacing between elements, and $\Delta\phi$ is the phase difference between elements. Figure 4a illustrates the near-field electric field distribution when elements are in-phase and Figure 4b illustrates the out-of-phase case.

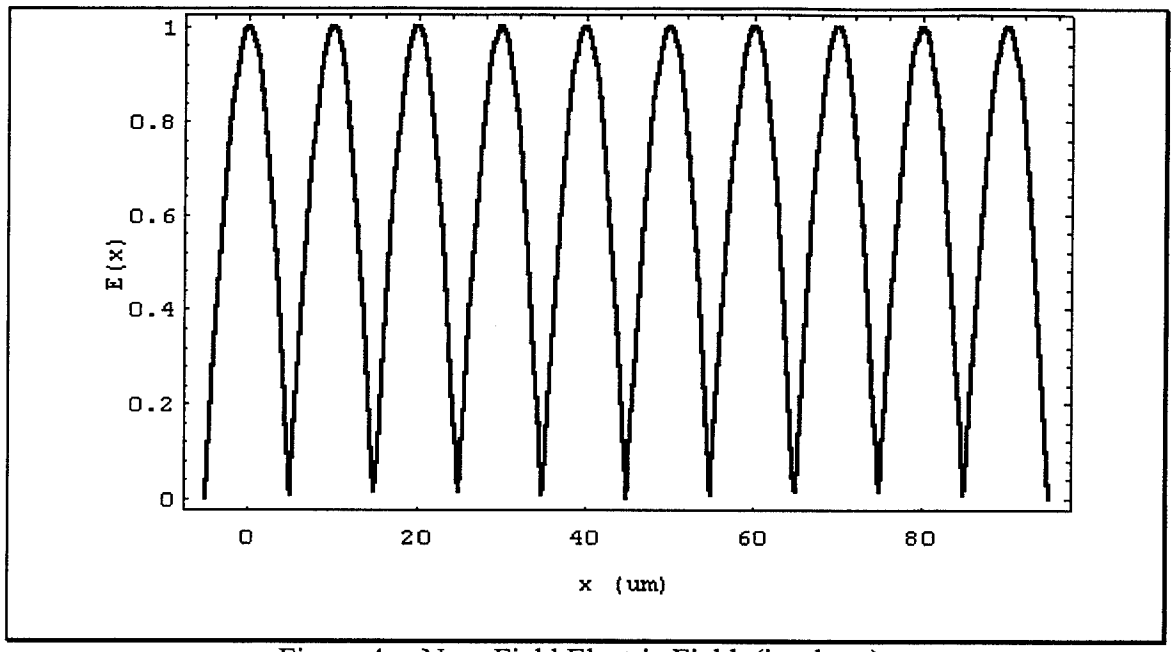

Figure 4a. Near-Field Electric Field (in-phase).

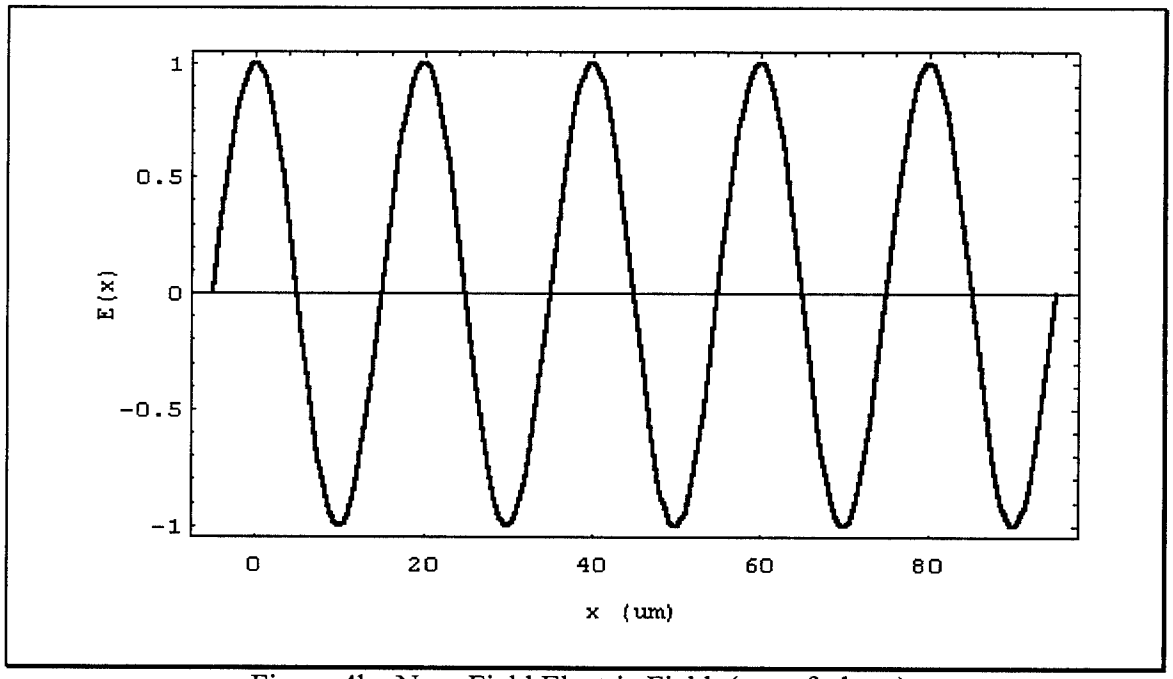

Figure 4b. Near-Field Electric Field (out-of-phase).

Simple diffraction theory predicts that the far-field electric field distribution of the LDA is proportional to the Fourier transform of the near-field electric field.[36] The electric field cannot be measured directly, but the intensity pattern can be. Intensity is proportional to $|\mathcal{F}\{E_{NF}(x)\}|^2$ where $\mathcal{F}$ is the Fourier transform operation evaluated at the spatial frequency $f_x \approx \theta/\lambda$, θ is the angular displacement from the center of the array, and λ is the wavelength of the field. Therefore:

$$I(\theta) \propto \left[\sin c\left(f_x b - \frac{1}{2}\right) + \sin c\left(f_x b + \frac{1}{2}\right)\right]^2 \cdot \left[\frac{\sin^2(5\Delta\phi - 10\pi f_x b)}{\sin^2\left(\frac{\Delta\phi}{2} - \pi f_x b\right)}\right] \tag{3.9}$$

using the same notation as Equation 3.8. This equation is used to analytically predict the far-field patterns shown in Figure 5. In Figure 5a, $\Delta\phi = 0°$ and the far-field pattern is a single lobe. Meanwhile, in Figure 5b, $\Delta\phi = 180°$ and the far-field pattern exhibits two main lobes, spaced equidistant from the center of the pattern.

If N lasing elements were placed together such that no interelement coupling occurred, the LDA would operate incoherently and the resulting intensity would be $N \cdot |\mathcal{F}\{E_{NF}(x)\}|^2$ But when the array operates coherently, coupling between elements leads to a peak intensity that is much higher. In the calculations leading to Figure 5, $|E_{NF}(0)| = 1$ unit. As seen in Figure 5a, when the LDA operates in the in-phase supermode, the single lobe has an amplitude $\approx$ 162 units of intensity. In Figure 5b, the two main lobes each have an amplitude = 100 units of intensity. Therefore, the rectified in-phase LDA should exhibit the highest peak intensity in the far-field, with an amplitude approximately 1.62 × that of the peaks of the two lobed pattern.

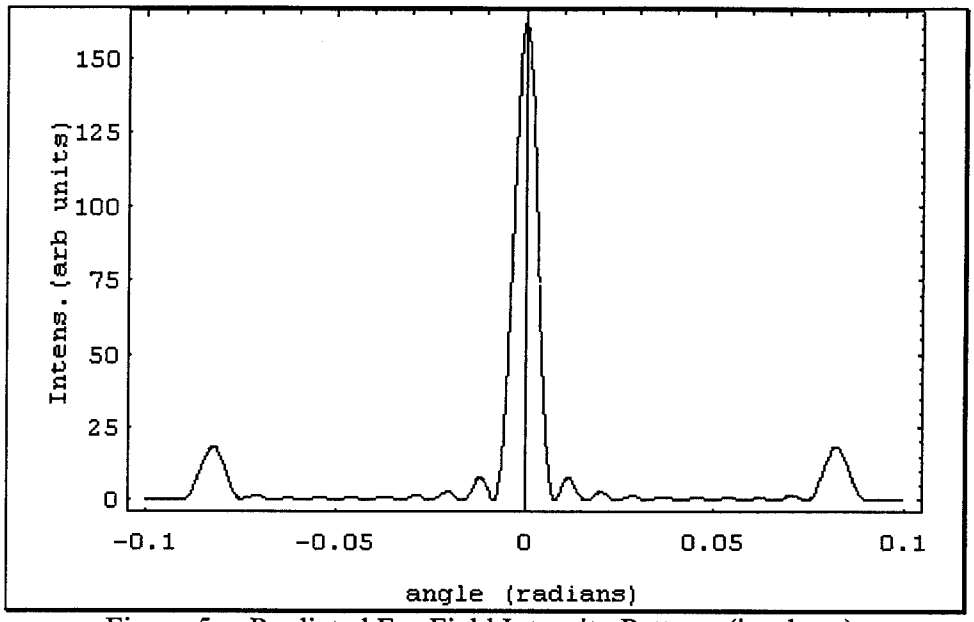

Figure 5a. Predicted Far-Field Intensity Pattern (in-phase).

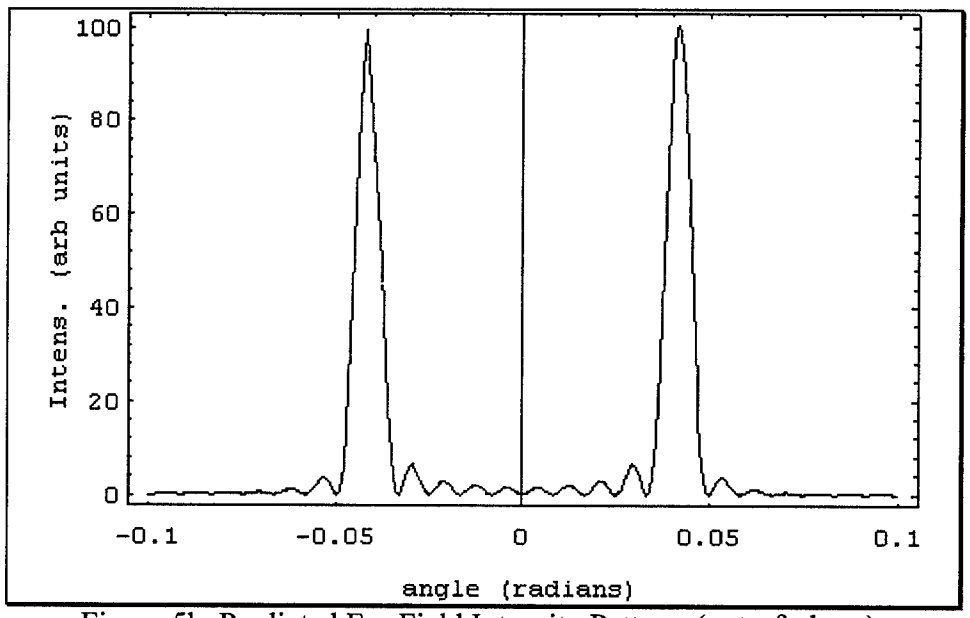

Figure 5b. Predicted Far-Field Intensity Pattern (out-of-phase).

Location of the Near and Far-Field Intensity Patterns

In order to characterize the LDA and control its output, it must be determined whether a location is in the near or far-field of the LDA when a measurement or observation is being made. Two cases must be considered. First, the LDA without optics, and second, the LDA when imaged through a lens.

When the laser is considered separately, the Fraunhofer approximation[36] can be used to determine when a location is in the far-field:

$$z >> \frac{k \cdot (x^2 + y^2)}{2} \tag{3.10}$$

where $k = 2\pi/\lambda$, and x and y are the length and width of the LDA elements. For the laser used in this experiment $x = 6$ μm and $y = 1$ μm. If much greater than is assumed to be 10 ×, an observation point is in the far-field when it is more than ≈ 1.4 mm from the LDA.

If a lens is used to image the laser intensity, the ray matrix method must be used to determine the location of the near and far-fields.[10] The relationship between an input ray from the LDA and the output ray from a lens can be written in matrix form:

$$\begin{pmatrix} x_2 \\ \alpha_2 \end{pmatrix} = \begin{pmatrix} A & B \\ C & D \end{pmatrix} \cdot \begin{pmatrix} x_1 \\ \alpha_1 \end{pmatrix} \tag{3.11}$$

which gives:

$$\begin{aligned} x_2 &= Ax_1 + B\alpha_1 \\ \alpha_2 &= Cx_1 + D\alpha_1 \end{aligned} \tag{3.12}$$

The transmission matrix contains three terms: translation from the lens to the observation plane, transmission through the lens, and translation from the LDA to the lens. The matrix is then:

$$\begin{pmatrix} A & B \\ C & D \end{pmatrix} = \begin{pmatrix} 1 & s \\ 0 & 1 \end{pmatrix} \cdot \begin{pmatrix} 1 & 0 \\ \frac{-1}{f} & 1 \end{pmatrix} \cdot \begin{pmatrix} 1 & d \\ 0 & 1 \end{pmatrix} = \begin{pmatrix} 1-\frac{s}{f} & s+d\cdot(1-\frac{s}{f}) \\ \frac{-1}{f} & 1-\frac{d}{f} \end{pmatrix} \tag{3.13}$$

where s = the distance from the lens to the observation point, f = the focal length of the lens, and d = the distance from the LDA to the lens. In the near-field, x_2 is independent of α_1. Therefore the location of the near-field is determined by setting matrix element B in equation 3.12 equal to 0 and solving for s:

$$s = \frac{d \cdot f}{d - f} \tag{3.14}$$

During the experimental portion of this work, f = 14.6 mm and d = 16.06 mm, so the near-field is <= 160.6 mm from the lens.

The far-field of the LDA after reflection by the micromirror array is then computed using the Fraunhofer approximation with x and y equal to the laser spot size at the mirrors. Therefore, any distance more than 140.4 mm from the micromirror array is in the far-field.

Measurement of Phase Difference

A key property of the LDA to be measured during characterization is the phase difference ($\Delta\phi$) of the electric field between adjacent elements. These measurements will be used to determine initial positioning of mirrors during the experimental phase.

Since the LDA is coherent, a two slit diffraction experiment can be used to measure $\Delta\phi$. The near-field of the LDA will be magnified and imaged onto a slide containing slits

of various widths and spacing. The slide is aligned so that only the light from the two LDA elements of interest is transmitted. The relative phasing can be determined by the position of the fringes under the diffraction envelope.

A fringe maximum occurring at the center of the diffraction envelope indicates that the two elements being transmitted are in-phase (i. e. $\Delta\phi = 0°$). Conversely, a fringe minimum occurring at the maximum of the diffraction envelope indicates $\Delta\phi = 180°$ between the elements being examined.[37]

Analytically, this can be seen from the equation for two slit diffraction:

$$I(\theta) = 4I_0 \, \mathrm{sinc}^2(\beta)\cos^2(\alpha) \tag{3.15}$$

where $\alpha = (ka/2 + \Delta\phi/2)$, $\beta = (kb/2)\cdot\sin(\theta)$, $k = 2\pi/\lambda$, a = slit spacing, and b = slit width. The sinc squared term is the same as the equation for single slit diffraction, and the cos squared term is due to the interference between slits. Figure 6 illustrates the diffraction patterns with $\Delta\phi$ equal to 0°, 90°, and 180° respectively.

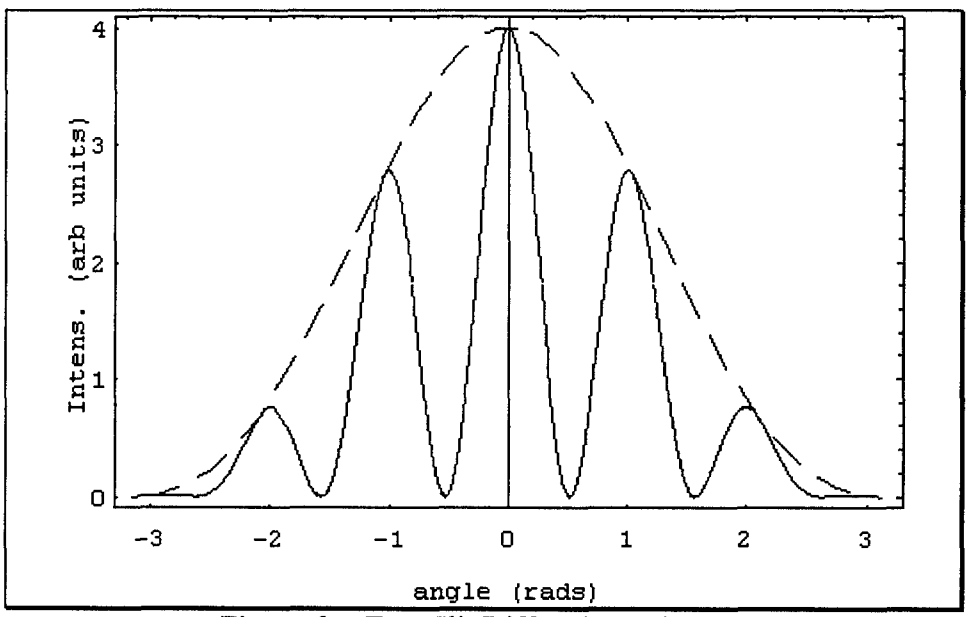

Figure 6a. Two Slit Diffraction, $\Delta\phi = 0°$.

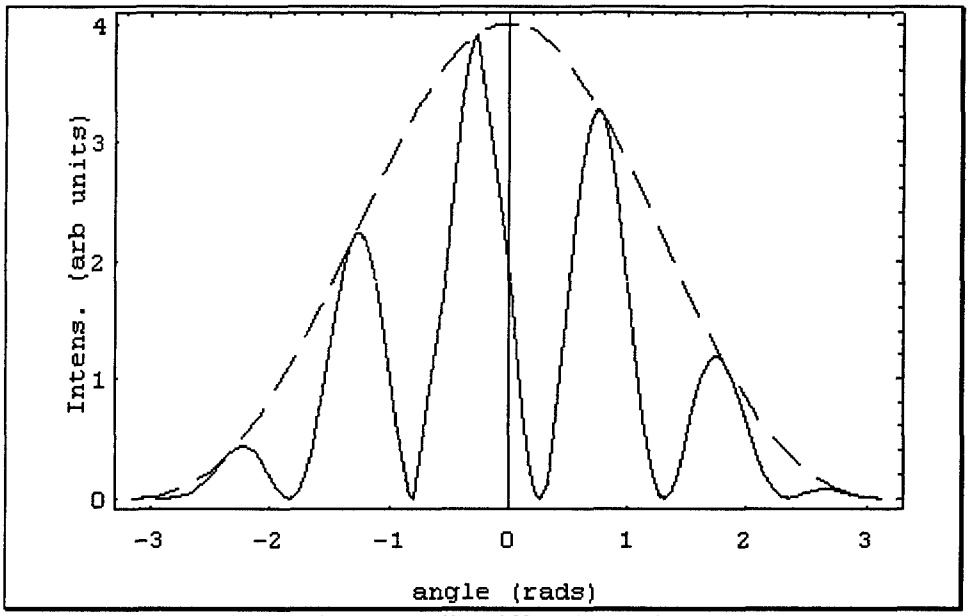

Figure 6b. Two Slit Diffraction, $\Delta\phi = 90°$.

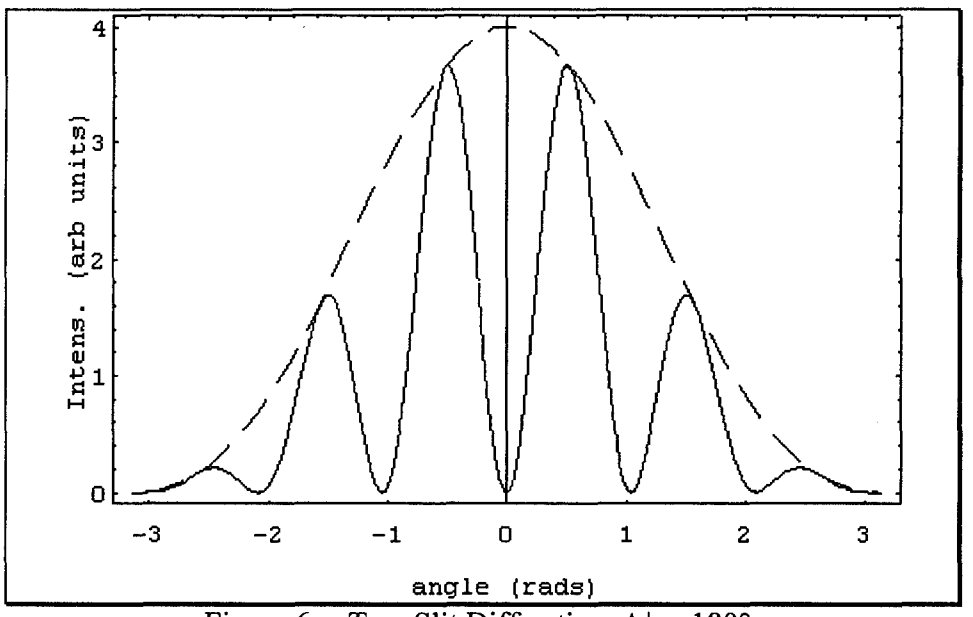

Figure 6c. Two Slit Diffraction, $\Delta\phi = 180°$.

Single Lobe in the Far-Field

The LDA to be used is in this experiment has ten elements with dimensions: 1 μm high × 6μm wide × 250 μm long. The interelement spacing is 10 μm. This LDA operates in a stable out-of-phase ($\Delta\phi = 180°$) supermode. Therefore, the LDA should exhibit a dual lobed far-field intensity pattern.

In the experiments to be performed, one of the key objectives is to obtain a single lobe in the far-field. Ideally, this lobe should contain as much of the total LDA power as possible. To attain this objective, the near-field of the LDA will be imaged onto the micromirror array so that the image is magnified 10 ×. A 10 × microscope objective will be used as the lens for imaging. The micromirror array was fabricated with this plan in mind, and so the individual mirrors are 60 μm across with center-center spacing of 100 μm. A more detailed description and actual pictures of the array can be found in Appendix A. Careful alignment of the optics will result in each individual emitting element being imaged onto a separate mirror.

Once each element is focused onto its own mirror, the OPD between each of the mirrors can be adjusted independently. Prior to this portion of the experiment, the mirrors have been characterized, $\Delta\phi$ between LDA elements has been measured, and λ of the LDA has been determined. Assuming for the moment that $\Delta\phi$ is 180°, and $\lambda = 828$ nm, the mirror voltages are set so that every other mirror is deflected $d = \lambda/4$ from its rest position. This gives an OPD = $\lambda/2$ between adjacent elements, introducing a phase

change of 180°. Thus, the light from the ten elements of the LDA will leave the mirrors in-phase and produce the desired single lobe intensity pattern in the far-field.

Phase Steering Theory

After obtaining the single lobed pattern, the next objective is to steer the beam electronically. Beam steering theory is analogous to the theory used to steer phased array radars. In phased array radar, the radiation pattern is shaped to point in the desired direction by imposing a planar phase front normal to the direction of the desired beam. The phase front is created by adjusting phase shifters to set an incremental phase difference (ψ) between adjacent elements of the array. The amount of phase difference is determined by:[38]

$$\psi = kb \sin\theta \tag{3.16}$$

where $k = 2\pi/\lambda$, λ is the wavelength of the electromagnetic radiation, b is the separation between elements, and θ is the desired steering angle. The maximum possible steering angle occurs when $\psi = 360°$, therefore $\theta_{MAX} \approx \lambda/b$ (radians). The micromirror array is already being employed as a phase shifter for the LDA, so application of the method is straight forward. In this scenario, the mirrors are acting as the emitters, $b = 100\ \mu m$, and the maximum steering angle is ≈ 8.29 mrad = 0.475°.

To steer the beam, one mirror is chosen as a reference point, the adjacent mirror is shifted by ψ, the next by 2ψ, etc. To minimize the amount of deflection required on the end mirrors, Mirror 6 (M6), near the center of the array, was chosen as the reference

point. M6 is left un-shifted, and the other mirrors are adjusted to obtain the required phasing. To steer the beam up, (θ negative) the mirrors are set according to Table 1:

Table 1

Beam Steering Phase Settings

Mirror	Phase	Mirror	Phase
1	$\pi - 5\psi$	6	0
2	-4ψ	7	$\pi + \psi$
3	$\pi - 3\psi$	8	2ψ
4	-2ψ	9	$\pi + 3\psi$
5	$\pi - \psi$	10	4ψ

The π phase shift on the odd numbered mirrors is the original phasing applied to put the elements all in-phase, and so must be included here. To steer the beam down, (θ positive) simply reverse the $\pm$ signs in Table 1. Steering is referred to as up and down in this configuration due to the orientation of the LDA. The steering angle is measured from the center of the uncorrected LDA intensity pattern.

Since the element to element phase shift across the array is a constant, Equation 3.9 can be used to predict the far-field intensity pattern. This equation predicts the presence of unwanted peaks, known as side lobes, in the intensity pattern. Phased array theory dictates that complete control of amplitude and phase are required to obtain the best fit to a desired radiation pattern. Amplitude control of individual LDA emitters is not possible. As a consequence, side lobes will be present in the far-field radiation pattern.

IV. Experiments and Results

Characterization of the Laser Diode Array

The laser diode array (LDA) used in these experiments is a commercial GaAlAs, ten element, gain-guided laser. (Spectra Diode Laboratories, Model SDL 2410-C, Serial Number P413). Each element of the array is $1 \times 6 \times 250$ μm. The center to center spacing of the elements is 10 μm. This gives an effective aperture size of approximately 1×100 μm. The elements of the array are evanescently coupled and operate in multi-longitudinal modes. The array is capable of generating up to 100 mW CW at room temperature in a stable two lobed far-field intensity pattern.[4]

Since this LDA will be used in all of the experiments to follow, it was characterized prior to use. Characterization was done for various input currents at room temperature. Average output power, power per far-field lobe, emission spectra, near-field and far-field intensity patterns, and two-slit diffraction patterns were observed and measured. From this data, lasing threshold current (I_{TH}), power efficiency, FWHM, angular separation between lobes, and phase difference between elements were determined.

Output Power and Current. The average CW output power of the LDA was measured as a function of input current. Input current was monitored with a Fluke Model 77/AN multimeter and power was measured using a Newport Model 815 digital power meter. From these measurements, I_{TH} was calculated to be 190 ± 2 mA. This is slightly higher than the manufacturer's stated value of 187 mA, probably due to the fact that the

LDA is nine years old. As Figure 7 illustrates, above I_{TH} there exists a linear relationship between input current and average power. The differential power efficiency (η) of the LDA was calculated from the power versus current measurements as: $\eta = 0.56 \pm 0.01$ mW/mA. This value is within the range of 0.55 - 0.75 mW/mA reported by the manufacturer.

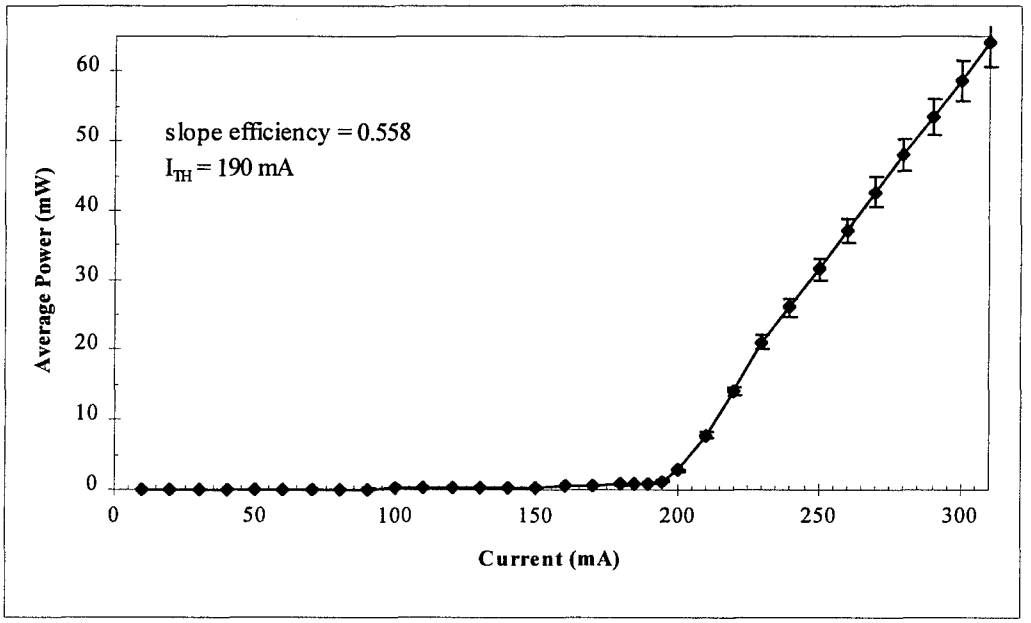

Figure 7. Average Output Power versus Current.

While observing line scans of the far-field intensity, it was noted that one lobe appeared to be stronger than the other. Therefore, measurements were performed to determine the relative amount of power in each of the far-field lobes. In general, the right lobe was slightly stronger, containing up to 57% of the total laser power at low currents. At higher currents, the power was more evenly divided with the right lobe containing 51% of the total power at 240 mA. The results are summarized in Table 2.

TABLE 2

Relative Power per Far-Field Lobe

Current (mA)	Total Power (mW)	Left Lobe Power (mW)	Right Lobe Power (mW)	Power Ratio Left / Right
205	1.42 ± 0.07	0.612 ± 0.03	0.812 ± 0.04	0.754
215	2.90 ± 0.15	1.24 ± 0.06	1.66 ± 0.08	0.747
225	5.51 ± 0.28	2.60 ± 0.13	2.90 ± 0.15	0.897
240	7.81 ± 0.39	3.78 ± 0.19	4.00 ± 0.20	0.945

Emission Spectra. The emission spectrum of the LDA was measured with an E. G. & G. Optical Multichannel Analyzer (OMA), Thermo Jarrel-Ash Model Number 12976300 Spectrometer, and an E. G. & G. Model 1471A Detector Interface coupled to an IBM compatible computer. OMA Vision Data Acquisition and Analysis software was used to capture, analyze and display the spectra.

Emission spectra was examined for input currents from 200 - 250 mA. The LDA required 15 - 20 minutes for the spectrum to stabilize after each current adjustment. This is because the laser is sensitive to the effects of drive current and temperature. Figure 8a shows the spectrum at 207 mA, with two dominant longitudinal mode lasing peaks at 828.15 and 828.45 nm. The center of the spectrum is at 828.32 nm and it's approximately 1.48 nm wide. At 225 mA, five lasing peaks are visible, as seen in Figure 8b. The peaks range from 827.46 to 828.87 nm, centered around 828.33 nm. The spectrum has broadened to about 2.25 nm. At 250 mA, there are only three resolvable peaks. Figure 8c illustrates the strong dominance of the center peak at 828.5 nm. The subordinate peaks are at 828.17 and 828.89 nm. The center of the spectrum is at 828.53 nm with a width of 2.31 nm.

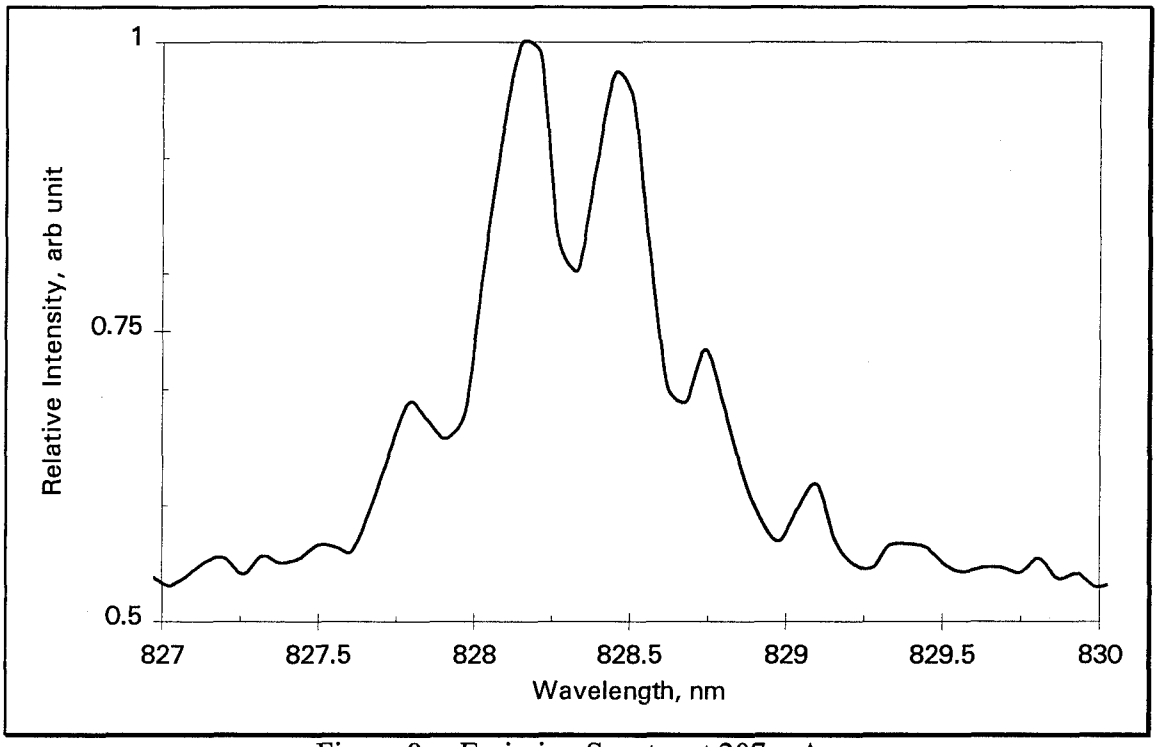

Figure 8a. Emission Spectra at 207 mA.

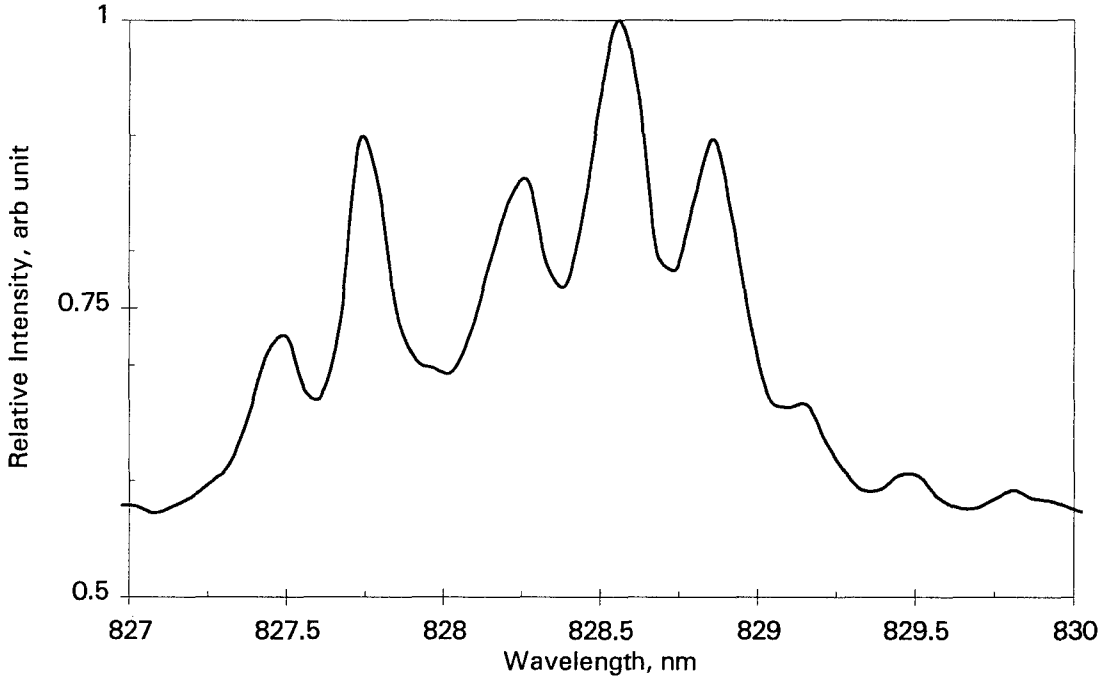

Figure 8b. Emission Spectra at 225 mA.

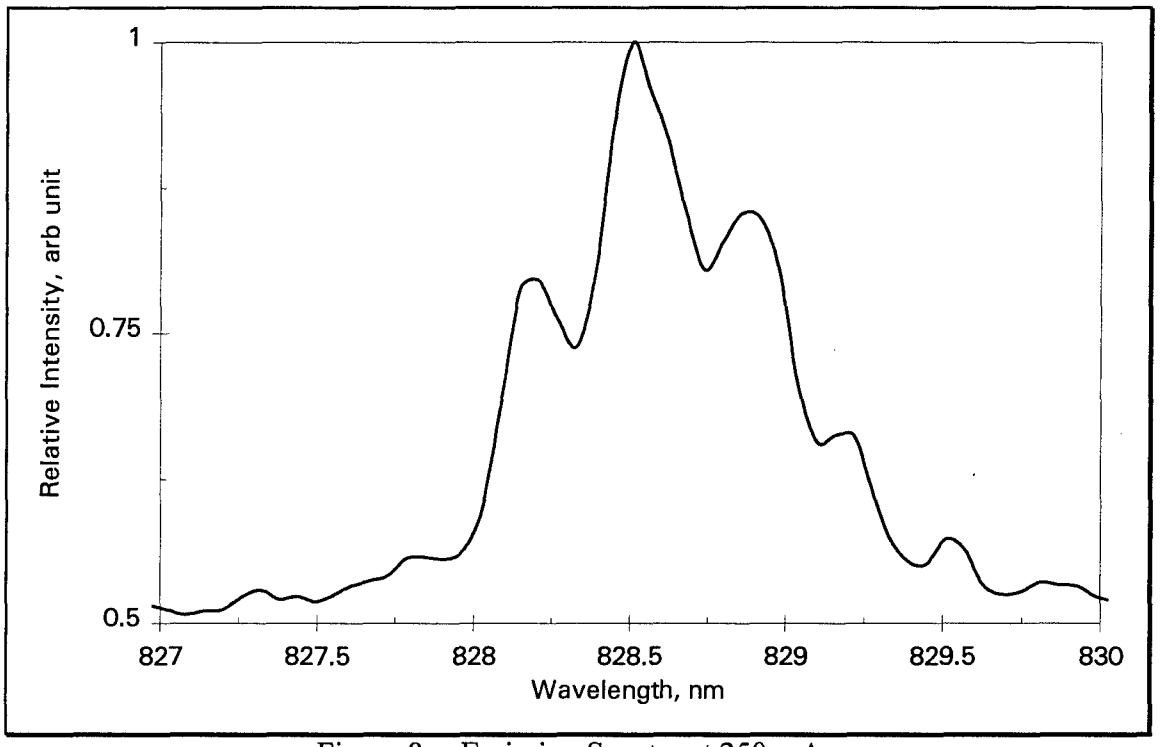

Figure 8c. Emission Spectra at 250 mA.

In all cases, as the current was increased, the spectrum broadened and the center of the spectrum shifted to longer wavelengths. This "red shift" is most likely due to heating effects of the LDA caused by the higher current. The array spectra also displayed periodic spacing between the different cavity longitudinal modes, $\Delta\lambda = 0.34 \pm 0.08$ nm. The analytically predicted value for $\Delta\lambda$ is given by[4]:

$$\Delta\lambda = \frac{\lambda^2}{2nd(1.25)} \tag{4.1}$$

where λ is the laser wavelength, n is the effective refractive index ($\approx$3.6), d is the length of the cavity ($\approx$250 μm), and 1.25 is the weighted dispersion of the semiconductor materials comprising the LDA as given by the operator's manual. This yields $\Delta\lambda = 0.31$ nm, comparable to the measured value.

According to the manufacturer, the wavelength of the LDA is 830 nm at 25° C. This translates to 828.33 nm when corrected for the lab temperature of 19.4° C during the spectra measurements.[4] The observed spectra therefore compares favorably with the manufacturer's specification. The difference between the two is well within experimental error.

Intensity Patterns. The near-field intensity pattern of the LDA was captured by a Sony CCD camera and displayed on a video monitor. The setup is shown in Figure 9. Line scans of the intensity pattern were made using ImagePro software.

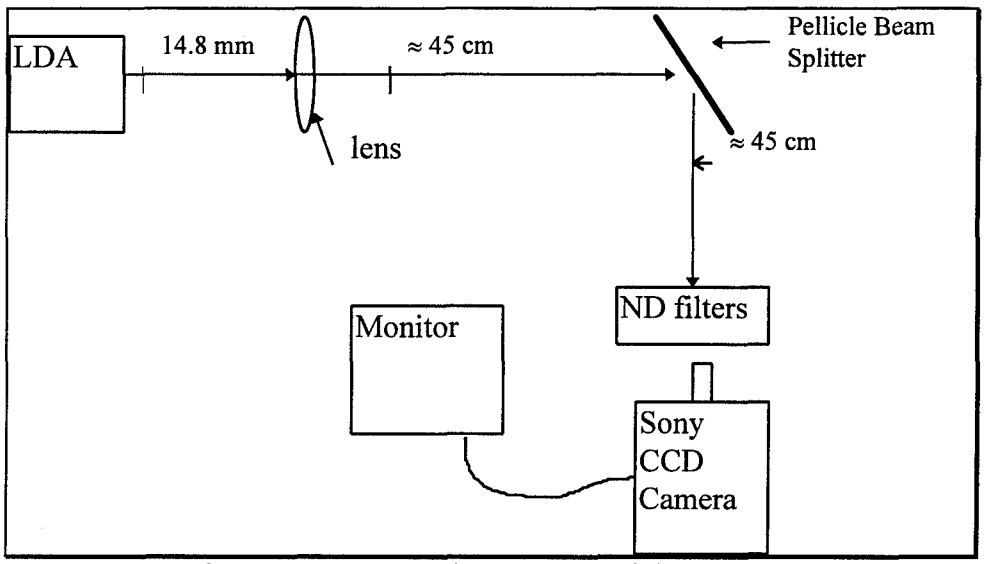

Figure 9. Setup to Observe Near-Field of LDA.

The near-field intensity pattern was observed by using a 10 × microscope objective as a lens. It was placed approximately 14.8 mm in front of the LDA, giving 60 × magnification of the near-field in the image plane, located approximately 90 cm from the lens. The pellicle beam splitter was used to reduce the laser intensity imaged onto the camera detector. The pattern is shown at 230 mA in Figure 10a. The ten separate emitting elements of the LDA are visible, the elements near the center of the array appear

to be stronger. The line scan in Figure 10b shows the relative intensity and spacing of the ten elements. The scan clearly shows the higher intensity of the center elements, and the semi-Gaussian radiation pattern of each element.

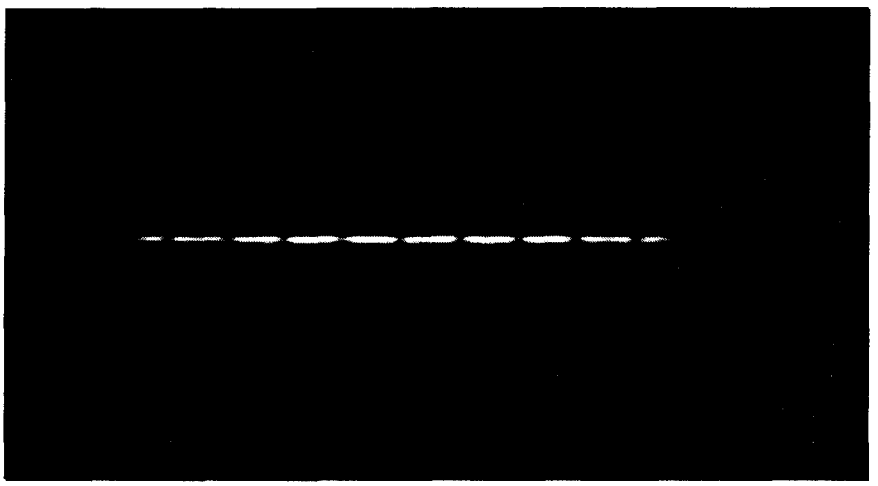

Figure 10a. Near-Field of Laser Diode Array.

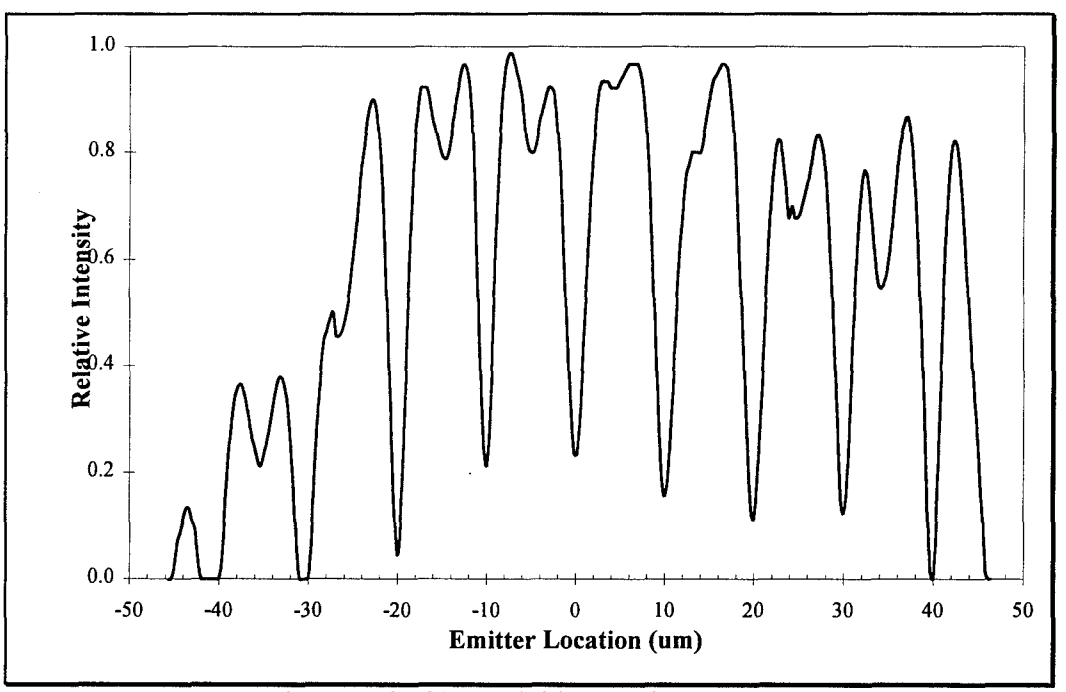

Figure 10b. Near-Field Intensity Pattern.

The far-field intensity pattern was observed by placing a General Electric TN2509 CID camera approximately 15 cm in front of the LDA with no optics in the beam path. Beamcode 5.0 software was used to capture and analyze the intensity pattern. The far-field shown in Figure 11a is significantly different than the near-field pattern. The pattern is dual lobed, indicative of a 180° phase difference between adjacent elements. The beam is very broad in the plane perpendicular to the junction, while not diverging as strongly in the plane parallel to the junction.

The far-field intensity pattern exhibits two distinct peaks. Figure 11b shows the intensity at 225 mA. From Figure 11, the amplitude ratio, lobe separation, and FWHM of the LDA can be measured. The two lobes are not of equal intensity, the average amplitude of the left lobe is 0.92 × that of the right lobe. The lobe separation on the graph is approximately 6.3°. The right lobe is not only higher in intensity, it is also broader. The FWHM is measured at 4.25° for the left lobe and 4.83° for the right lobe, these values are approximately ten times the diffraction limit of 0.475°.

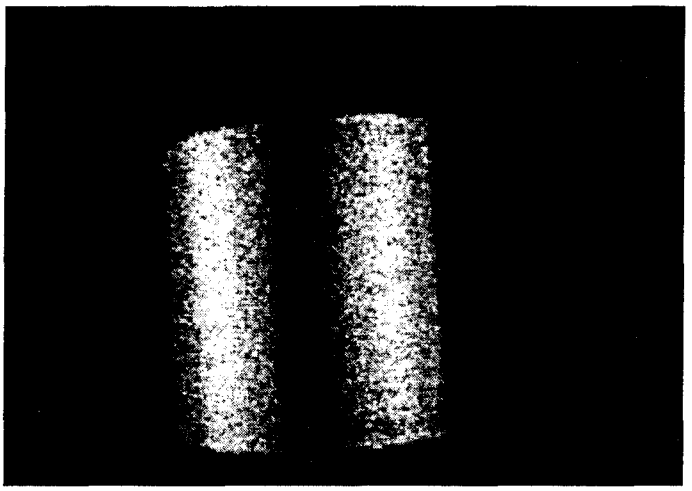

Figure 11a. Far-Field of Laser Diode Array.

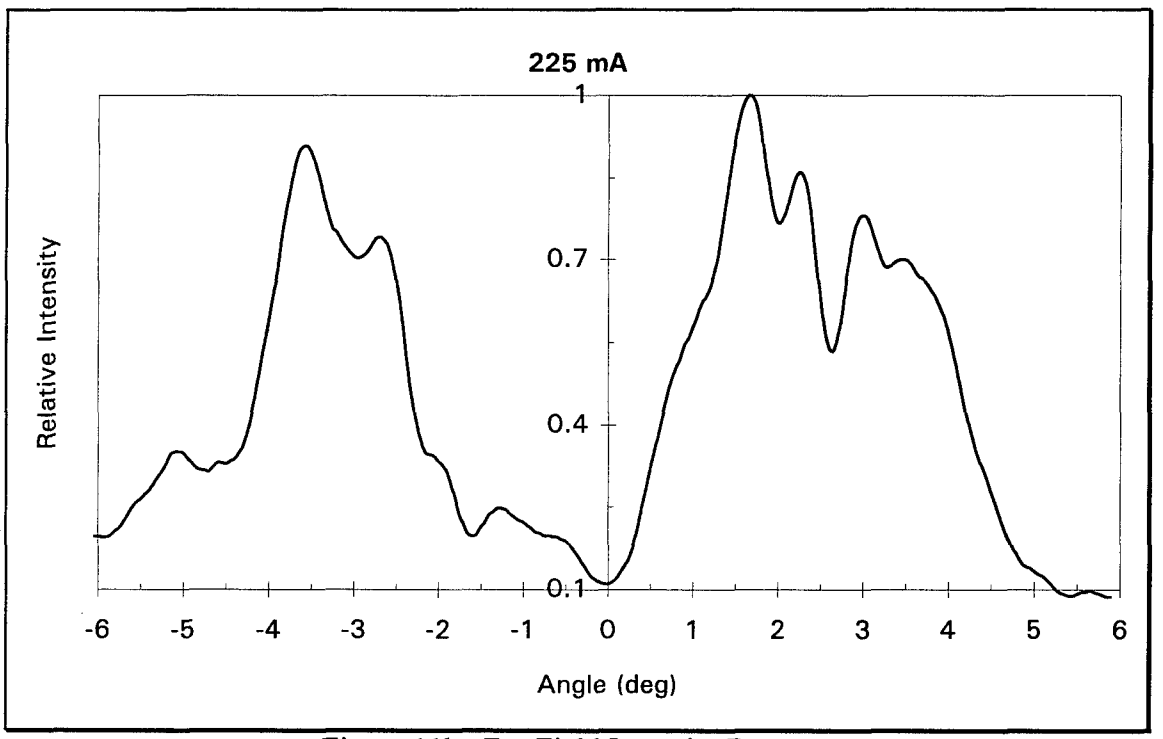

Figure 11b. Far-Field Intensity Pattern.

Lobe Separation and FWHM. The separation between the far-field lobes was calculated by measuring the distance (d) from the LDA to the viewing screen and measuring the separation (s) between the centers of the two far-field lobes. The angular separation (θ) of the lobes from the center of the pattern, is then given by:

$$\theta = 2\left[\tan^{-1}\left(\frac{0.5s}{d}\right)\right] \tag{4.2}$$

Lobe separation has been predicted theoretically by Streifer *et al.* via simple diffraction theory:[5]

$$\theta = 2*[\tan^{-1}(-\Delta\phi/kD)] \tag{4.3}$$

$\Delta\phi$ = the phase difference between elements (180°), $k = 2\pi/\lambda$, and D = separation between elements (10μm). This equation predicts a lobe separation of 4.75°.

The actual measured separation between far-field lobes was 6.26 ± 0.04° at 200 mA and increased with injection current to 6.42 ± 0.22° at 240 mA. The separation is considerably wider than the predicted value. This is because the simultaneous operation of several longitudinal array modes causes the beam to diverge. As injection current is increased, more longitudinal array modes are present, and the beams separate further. Figure 12 illustrates far-field patterns at 200 mA and 240 mA respectively. These images were captured using Beamcode 5.0, no optics, and the camera 15 cm in front of the LDA.

The far-field intensity graphs were also used to measure the FWHM of the lobes. As expected, increasing the current excited multiple array modes in the laser. This in turn caused the measured FWHM to increase. At all currents, the FWHM was many times the diffraction limit of 0.475°. FWHM measurements are tabulated in Table 3.

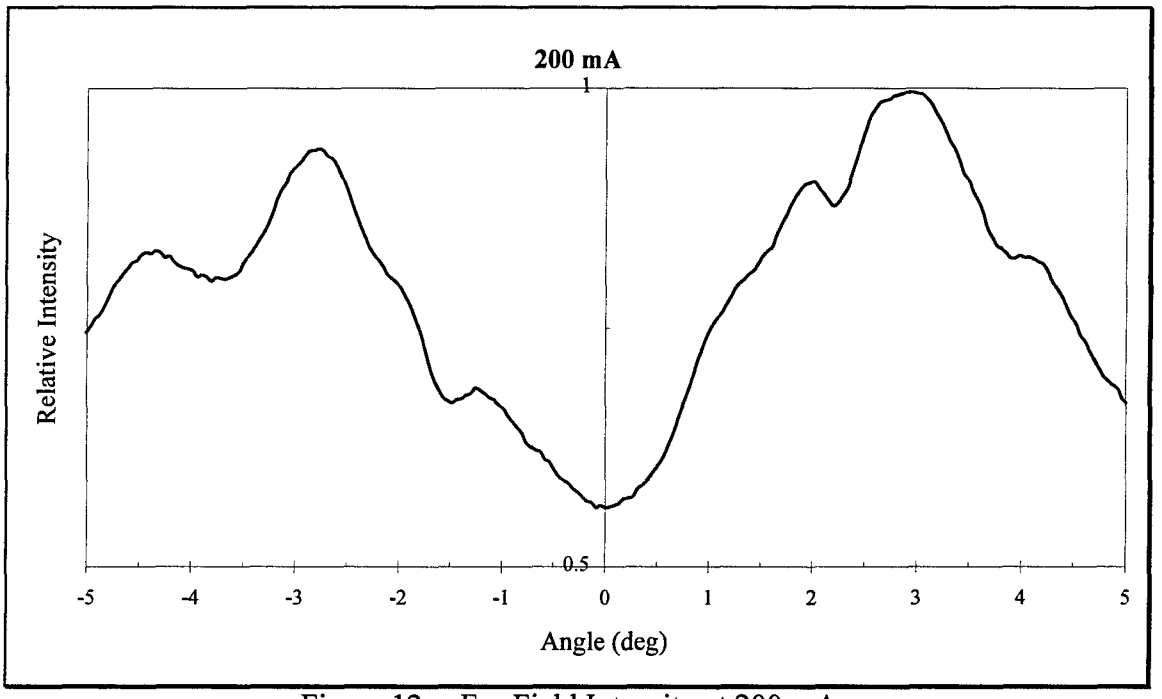

Figure 12a. Far-Field Intensity at 200 mA.

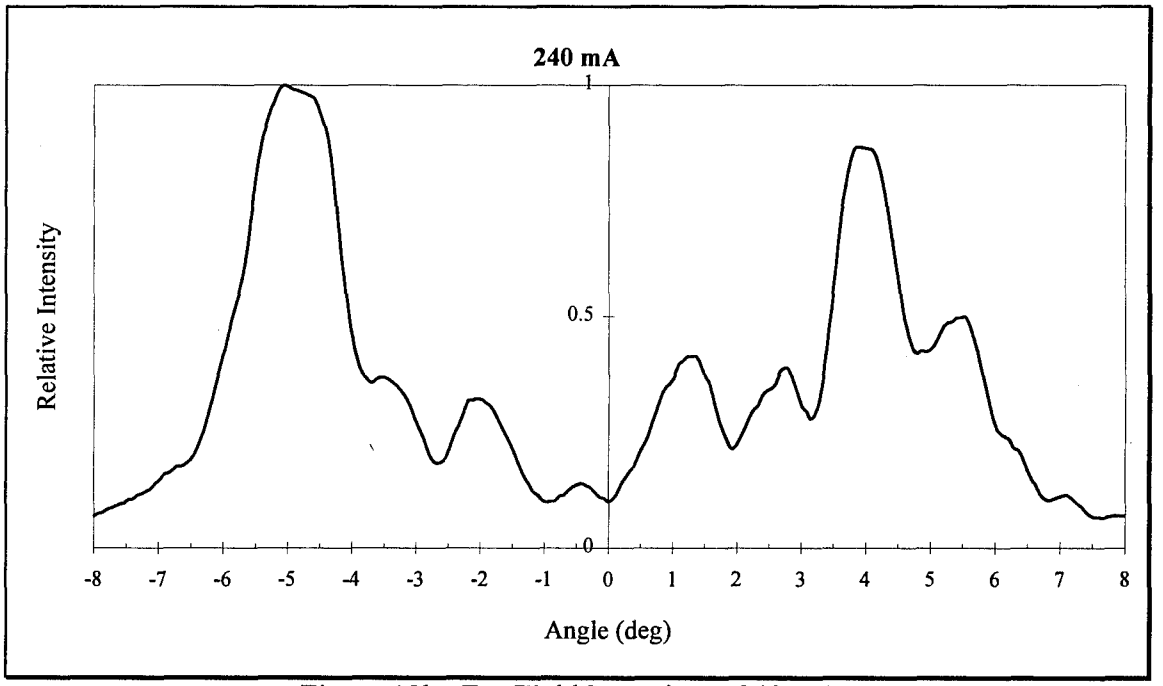

Figure 12b. Far-Field Intensity at 240 mA.

TABLE 3

FWHM Measurements

Current (mA)	Left Lobe Width °	Right Lobe Width °
200	2.57	3.00
205	3.43	4.62
215	3.60	4.30
225	4.25	4.83
240	4.46	5.46

Phase Difference. To measure the phase difference between adjacent elements, two slit diffraction was employed. As described in Chapter III, the diffraction pattern will depend on the phase between coherent sources illuminating the slits.

The LDA elements are imaged onto a slide containing two slits using a 10 × objective as a lens. The slits are each 40 μm wide and their center - center spacing is 125 μm. The LDA to lens distance is 15.2 mm and the lens to slide distance is 379.6 mm. The diffraction pattern is observed on a screen placed approximately 75 cm from the slits. The results are shown in Figure 13. In Figure 13a, both slits are illuminated by the same LDA element. A fringe maximum occurs at the center of the diffraction envelope, indicating that $\Delta\phi \approx 0°$. In Figure 13b, the slits are illuminated by two adjacent LDA elements. A fringe minimum occurs exactly at the center of the diffraction envelope, and the maxima are evenly displaced from the center. This pattern is caused by a 180° phase difference between the elements.

All adjacent elements were checked with the same results, $\Delta\phi = 180°$ in all cases. Therefore, as predicted, adjacent elements of the LDA are out-of-phase by 180°. This

verifies that the LDA is operating in the highest order supermode, n = 10.

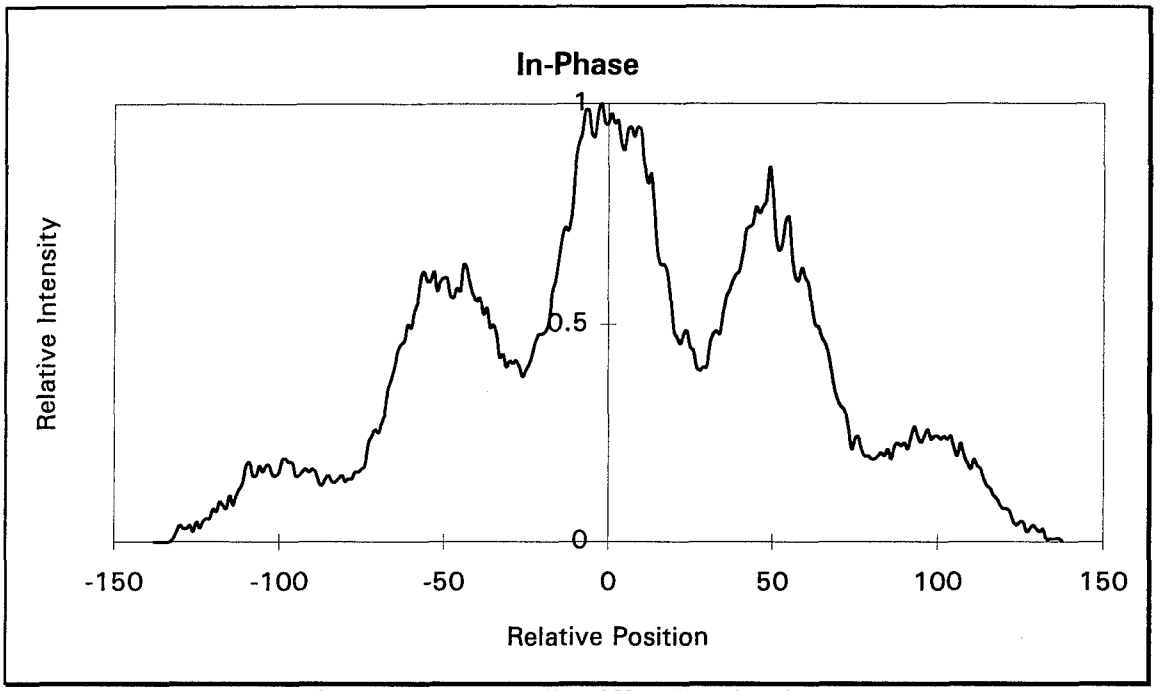

Figure 13a. Two Slit Diffraction, in-phase.

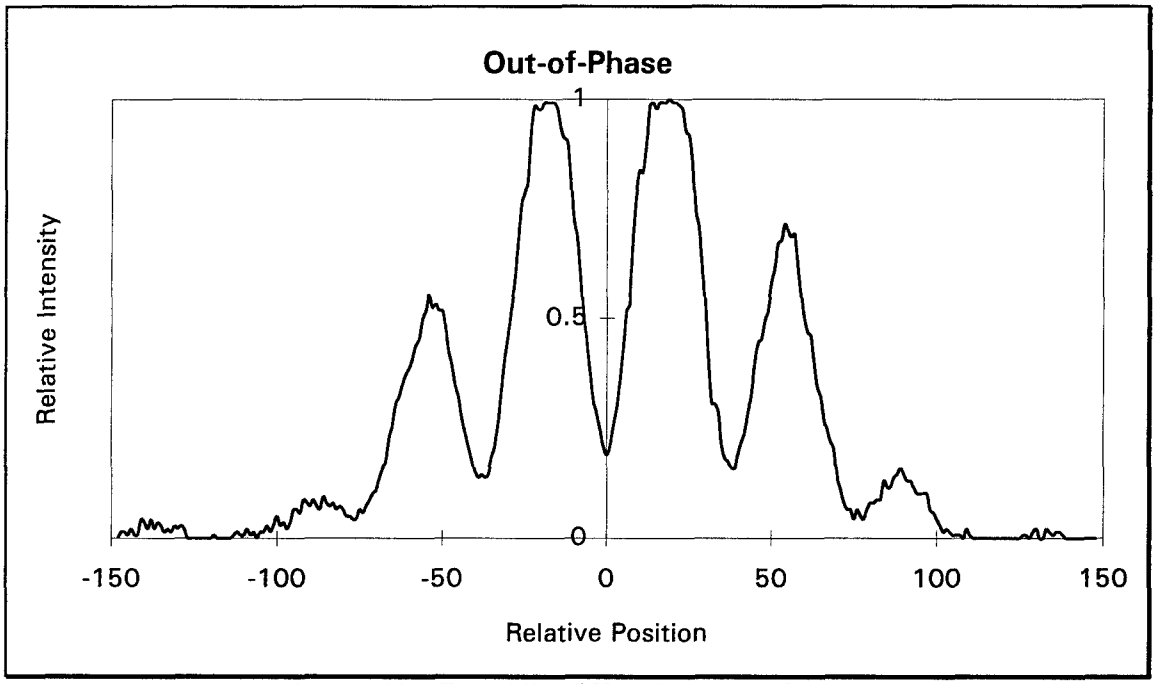

Figure 13b. Two Slit Diffraction, out-of-phase.

Characterization of the Micromirror Array

The micromirror array is at the core of these experiments. The array is shown in Figure 14. Accurate alignment of mirrors will be crucial to creating the proper phasing of the LDA for a single lobe in the far-field and for steering the lobe. Therefore, each individual mirror was tested to measure its deflection when a D. C. voltage was applied. The reflectivity of the mirrors was also measured.

Mirror Deflection Versus Voltage. The theory used to perform this experiment is detailed in Chapter III. The intensity of a reflected interference pattern is measured as the applied voltage varies, and from these measurements, the phase difference and hence mirror deflection could be calculated. The micromirrors required a dry and relatively dust free environment to work properly. Since the mirrors are actuated by electrostatic attraction, if the laboratory was humid, water saturated dust particles were attracted to the mirror when the voltage was applied. Due to their small size, even a small speck of dust could cause the mirrors to stick or be shorted out. To prevent this, a tent was constructed around the mirrors. Nitrogen was pumped into the enclosure during testing to create a dry dust free environment for the mirrors.

A deflection as a function of voltage calibration chart was generated for each of the ten mirrors. Quite a difference in response was noted from one mirror to the next. 207 nm of mirror deflection is needed to create a 180° phase shift of the laser. To obtain a 207 nm deflection required anywhere from 12.25 to 22 volts for nine of the ten mirrors. The average voltage for 207 nm deflection was 19.25 volts. The chart for M6 indicated

that this mirror required 29 volts to reach 207 nm. It is possible that the mirror was sticking or had a speck of dust lodged under it. The mirror was suspected of being bad, so it was left grounded and was not deflected throughout the remaining experiments. At 30 volts, mirror deflection ranged from 550 - 827 nm, except for M6. Therefore, all of the mirrors except M6 were capable of producing 360° of phase shift. Table 4 compares the voltage differences between mirrors for several deflection distances, and Figure 15 shows a comparison of mirror deflection versus voltage curves.

Measurement of Mirror Reflectivity. The reflectivity of the mirror array was determined by measuring the power of the LDA exiting the 10 × objective, and measuring the power of the far-field pattern created by the mirrors. The reflectivity was expected to be quite high since the mirror faces are gold and chromium plated. But, on average, only 43.6% ± 0.9% of the LDA power was reflected by the mirrors into the far-field pattern. Several loss mechanisms were present to account for this low reflectivity. Losses were due to holes in the center of the mirrors and imperfect alignment between the mirrors and the LDA elements. As can be seen from Figure 10a, the elements of the LDA appear not to be exactly the same size and spacing due to uneven illumination of the elements. This made alignment difficult, some elements appeared to be centered on a mirror, while other elements appeared to be off to one side or the other. Also, at higher currents, the LDA appears to overfill the mirrors. The light that falls outside the mirror face is reflected by the mirror flexures or array substrate or diverges away. These effects result in lower reflectivity and unwanted noise in the far-field intensity pattern.

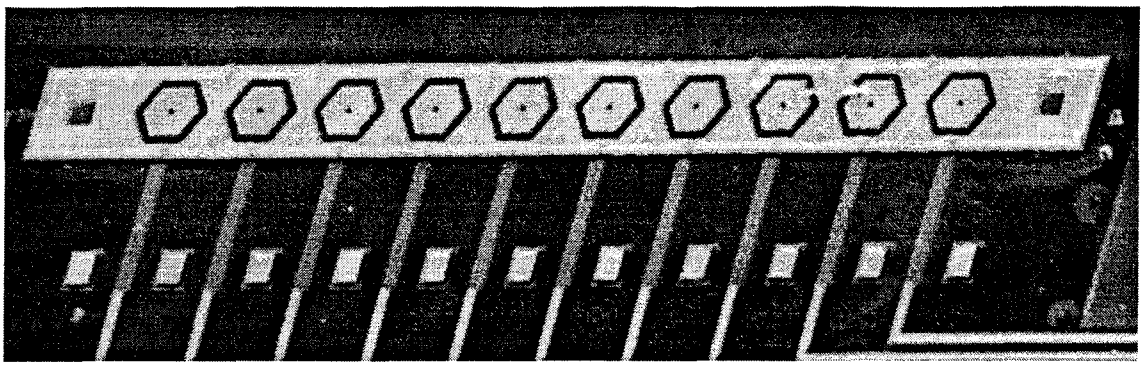

Figure 14a. Photograph of the Micromirror Array.

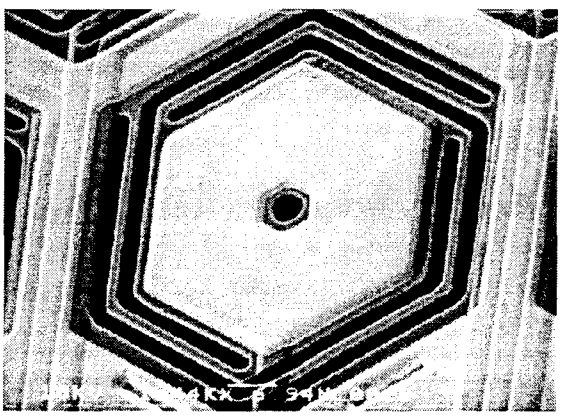

FIGURE 14b. Photograph of a Single Mirror to Show Detail

TABLE 4

MIRROR DEFLECTION COMPARISON

Mirror	Voltage for 207 nm Deflection	Deflection (nm) at 15 V	Deflection (nm) at 30 V
M1	18.25 ± 0.5	153 ± 3	550 ± 15
M2	11.50 ± 0.5	284 ± 3	827 ± 15
M3	21.50 ± 0.5	76 ± 3	498 ± 15
M4	19.00 ± 0.5	173 ± 3	604 ± 15
M5	15.50 ± 0.5	199 ± 3	671 ± 15
M6	29.0 ± 1.0*	72 ± 3*	222 ± 15*
M7	19.75 ± 0.5	118 ± 3	633 ± 15
M8	20.00 ± 1.0	125 ± 3	585 ± 15
M9	22.00 ± 0.5	79 ± 3	609 ± 15
M10	18.25 ± 0.3	140 ± 3	637 ± 15

*M6 suspected to be bad.

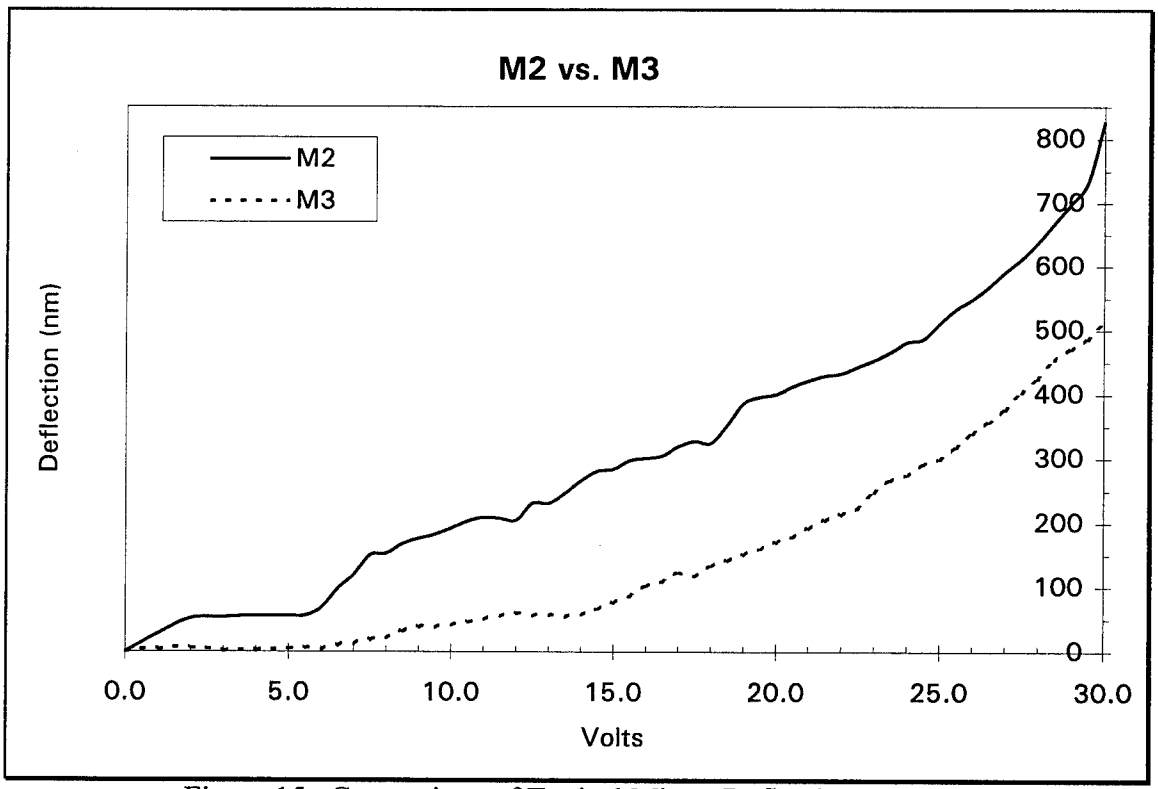

Figure 15. Comparison of Typical Mirror Deflection Curves.

Single Lobe in the Far-Field

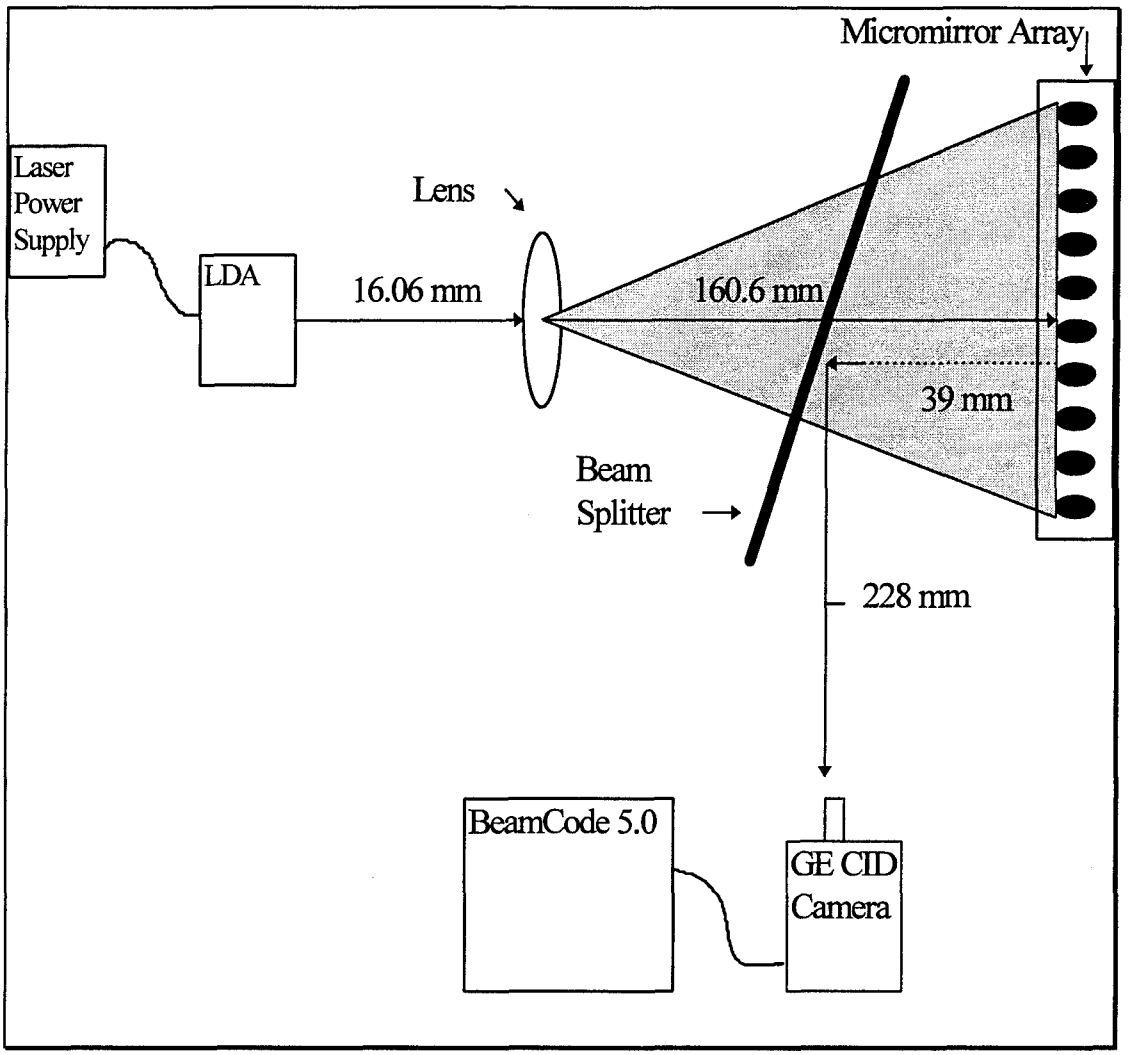

Figure 16. Experimental Setup.

Figure 16 shows the setup used to obtain and observe a single lobed far-field intensity pattern. The near-field of the LDA is imaged onto the micromirror array through a 10 × microscope objective placed 16.06 mm from the front of the LDA. The micromirror array is at the image plane of the lens, 160.6 mm from the lens. The alignment of the LDA, lens, and micromirror array is adjusted so that each element of the LDA is imaged onto a micromirror. The alignment of the LDA elements onto the mirrors is monitored

via a 7× microscope equipped with a CCD camera (not shown). The LDA radiation is reflected from the mirrors to the beam splitter, which directs the radiation to the CID camera. The camera is placed so that the micromirror to camera distance, via the beam splitter, is 267 mm. The camera captures the far-field intensity pattern which is monitored with Beamcode 5.0 software.

All the intensity patterns during the next two experiments were observed with the General Electric TN2509 CID camera and Beamcode 5.0 software. This package provides simultaneous intensity patterns and line scans of the laser pattern. The effects of mirror adjustment on the far-field intensity pattern could then be monitored in real time.

The voltage to the mirrors is generated and controlled by a National Instruments Corp. AT-AO-6/10 analog output board mounted in an IBM compatible computer. The board is capable of generating ± 10 V.D.C. for each output channel. By setting Channel 0 to -10 volts and connecting it to the mirror ground, up to 20 volts can be applied to the mirrors. When more than 20 volts was needed a 9 volt battery was placed in series between the board and the mirror. M1, M3, M5, M7, and M9 were programmed for a 180° phase change, 207 nm of deflection from their respective charts. M2, M4, M6, M8, and M10 were grounded.

The LDA was set to 200 mA and aligned to the mirrors. A typical two lobed pattern was seen in the far-field on the Beamcode monitor. When the voltage was turned on, the two lobes moved closer together. They overlapped, but didn't quite form a single lobe. The odd numbered mirrors were then adjusted one at a time while observing the intensity pattern. As the mirrors were adjusted, "lines" of intensity could be seen moving across

the monitor. The mirrors were adjusted so that the best possible single lobe pattern was obtained, and the voltages were recorded. Table 5 shows the predicted voltages and the actual voltages used to achieve a single lobed far-field pattern.

TABLE 5

Single Lobe in the Far-Field

Mirror	Predicted Voltage	Actual Voltage at 200 mA	Actual Voltage at 210 mA	Actual Voltage at 225 mA	Actual Voltage at 240 mA
1	18.25	19	19	19	18
3	21.6	22.5	22	25	23
5	15.5	21	21	22	15
7	19.75	15	9	9	9
9	22	19	19	13	9

The voltage to M1 never had to be varied more than 1 volt from its predicted value, while M3 had to be set as high as 3.4 volts above its predicted value. M5 needed as much as 6.5 volts more than predicted, but based on the predicted and actual values of the other mirrors, 21 volts is not an unreasonable number. It is possible that the mirror's deflection chart was in error, or that its response had changed over time. M7 had to be set as much as 10.75 volts below its predicted value. On the first two attempts M9 only had to be adjusted to 3 volts below its predicted value, but much lower on the next two attempts to get the best far-field pattern. There are several possible reasons for the discrepancy between the actual and predicted voltages. One reason may be that the LDA and the micromirror array were not aligned perfectly parallel to each other. If the micromirror array was tilted so that the mirrors were not all equidistant from the LDA to begin with, some phasing has already been introduced before the mirrors are moved. This theory is supported by the fact that the single lobe is steered approximately 0.1° from the center of

the pattern. Another possibility is that at their rest positions, the mirrors are not level with each other. When the mirrors were characterized, it was assumed that the mirrors all returned to the same level when the voltage to them was removed. Slight variations in the manufacture of the mirror flexures could result in the mirrors not all being the same distance above the array substrate at rest.

Figure 17 shows the single lobe patterns obtained for LDA currents of (a) 200 mA, (b) 210 mA, (c) 225 mA, and (d) 240 mA. All the single lobe patterns were steered slightly to the right of center. The mirror voltages required only minor adjustments to optimize the single lobe patterns as the injection current was increased. Table 6 summarizes the results.

TABLE 6

Characterization of the Single Lobe in Far-Field

Input Current	Peak Offset (Degrees)	Amplitude Ratio	FWHM
200 mA	0.065°	1.60	0.167°
210 mA	0.107°	1.15	0.206°
225 mA	0.135°	1.45	0.240°
240 mA	0.133°	1.10	0.433°

The peak offset indicates how far off center the single lobe was. The amplitude ratio compares the amplitude of the single lobe to the average amplitude of the two lobes. From Chapter III, the expected amplitude ratio is approximately 1.62. FWHM is given in degrees, for comparison to the diffraction limit of 0.0475°. The FWHM exhibited the same behavior that was seen when characterizing the LDA. As the current increased, the intensity pattern broadened. The FWHM went from 3.5 × the diffraction limit at 200 mA

up to 9.1 × the diffraction limit at 240 mA. This result was to be expected since the LDA did not exhibit a diffraction limited far-field pattern when it was characterized.

The mirror voltages needed to obtain the best single lobe intensity pattern were recorded in Table 5. With a calibration chart generated in this way, a single lobe intensity pattern could be reliably obtained for a wide range of injection currents.

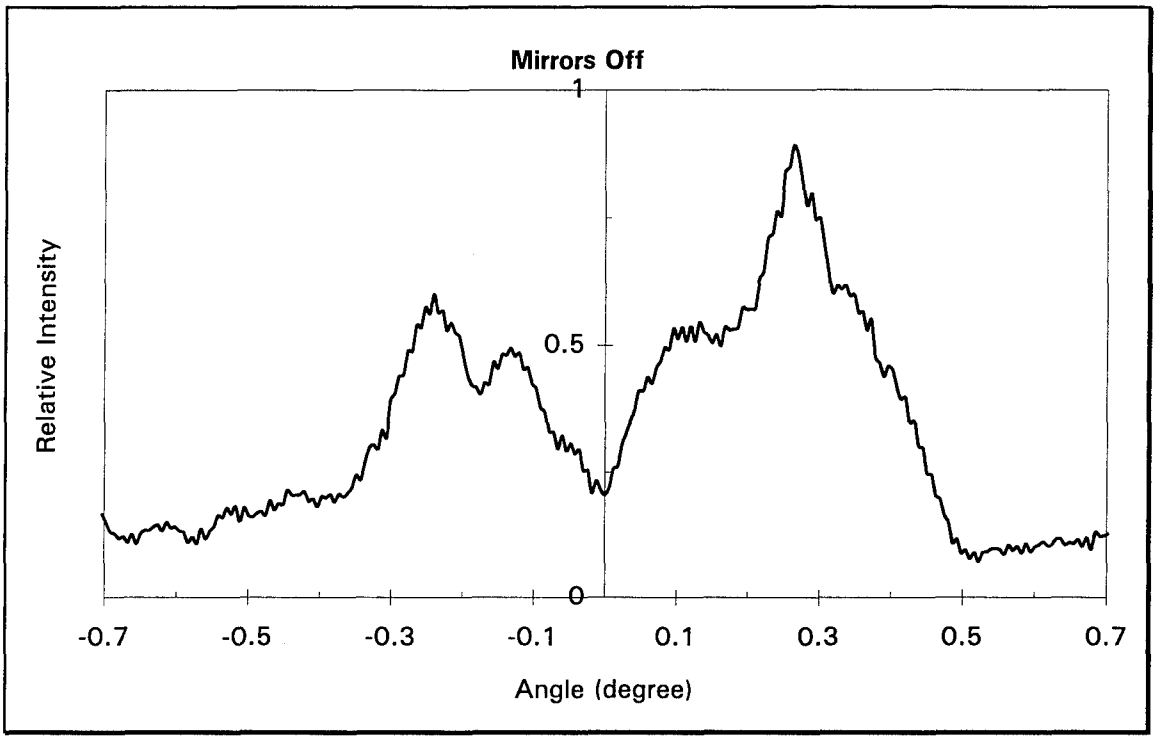

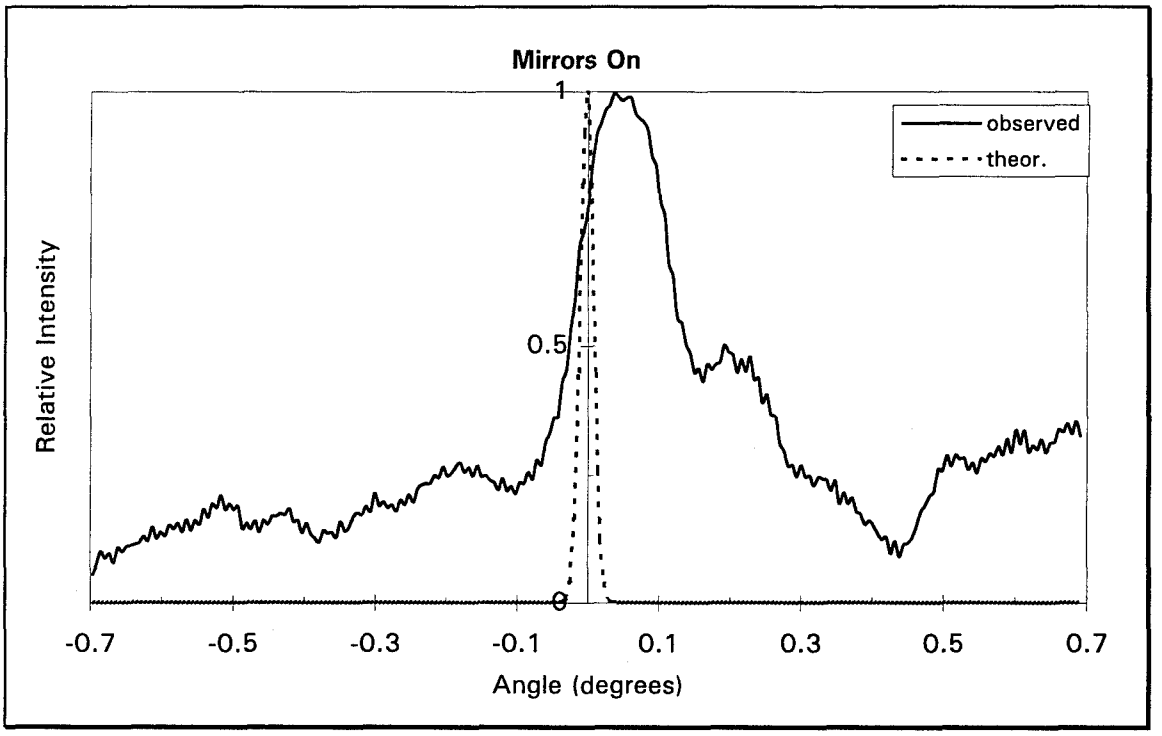

Figure 17a. Single Lobe in Far-Field (200 mA).

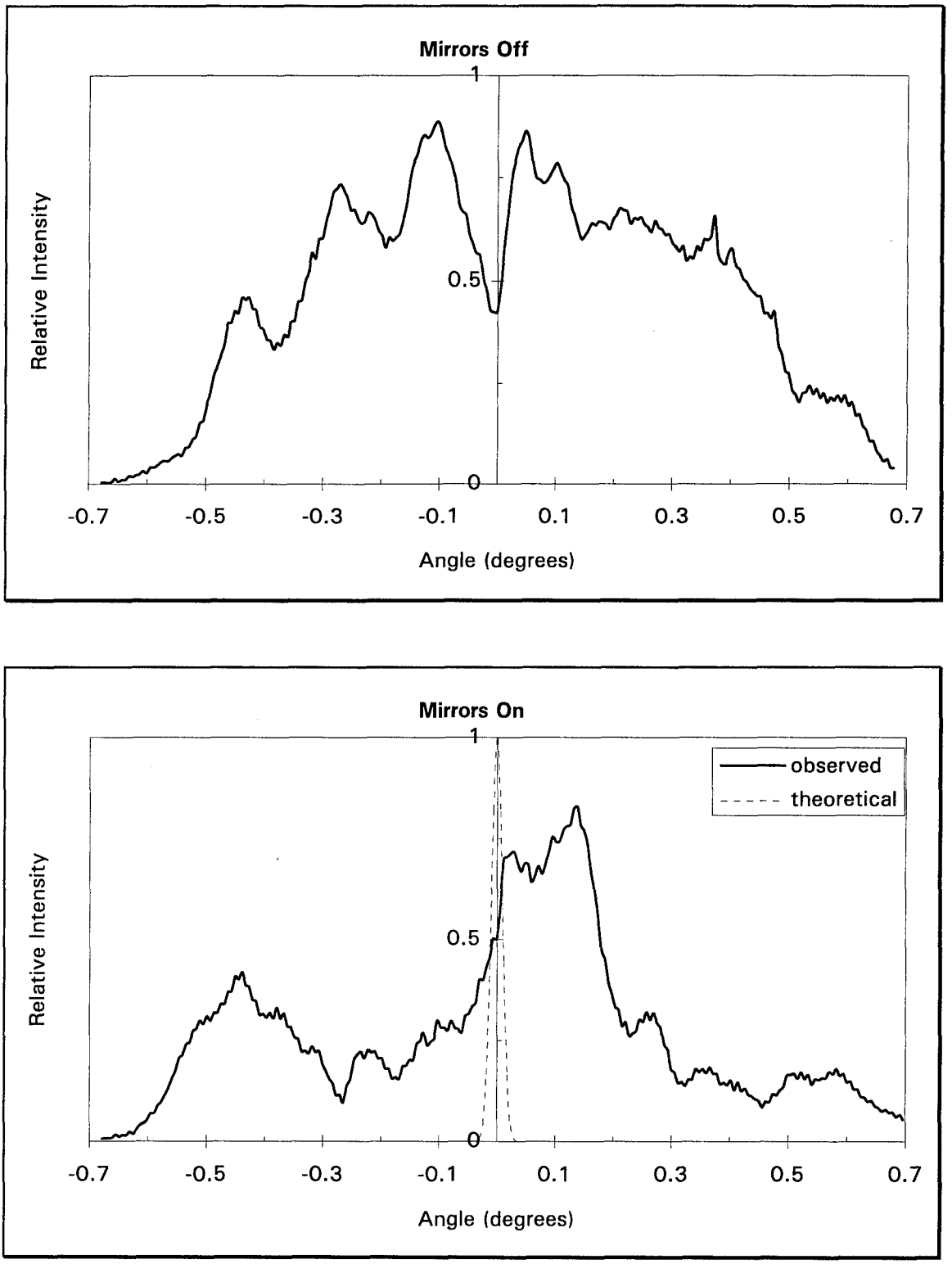

Figure 17b. Single Lobe in Far-Field (210 mA).

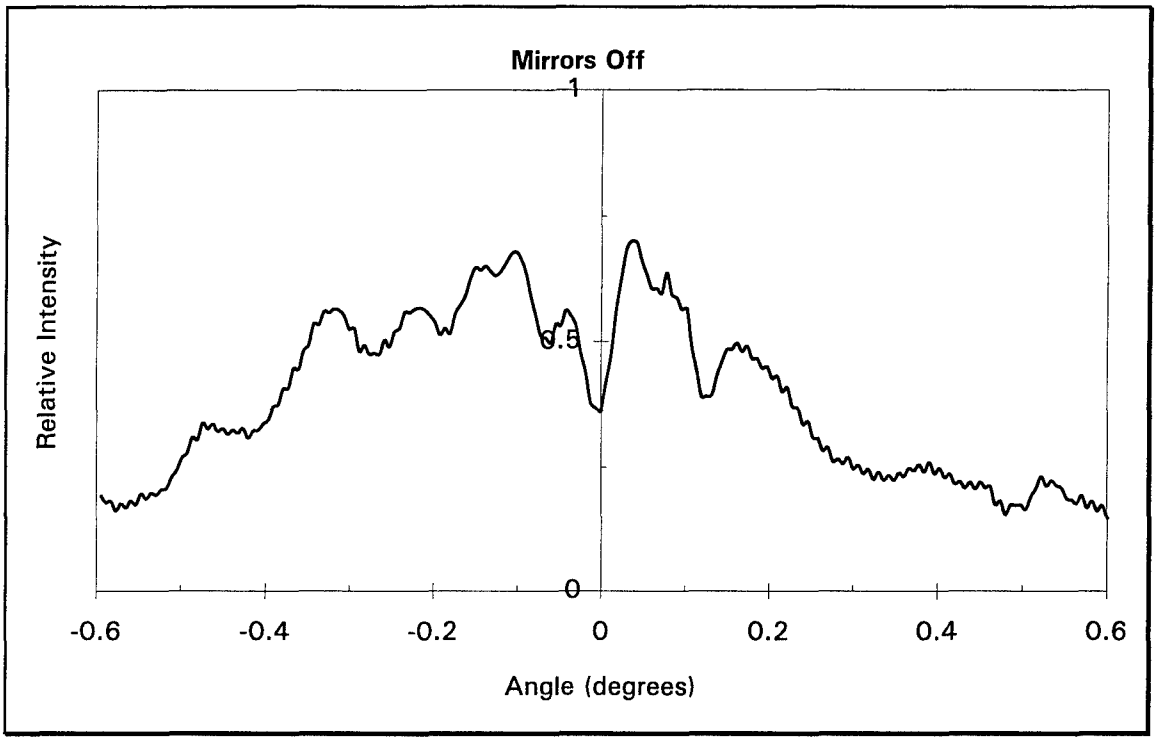

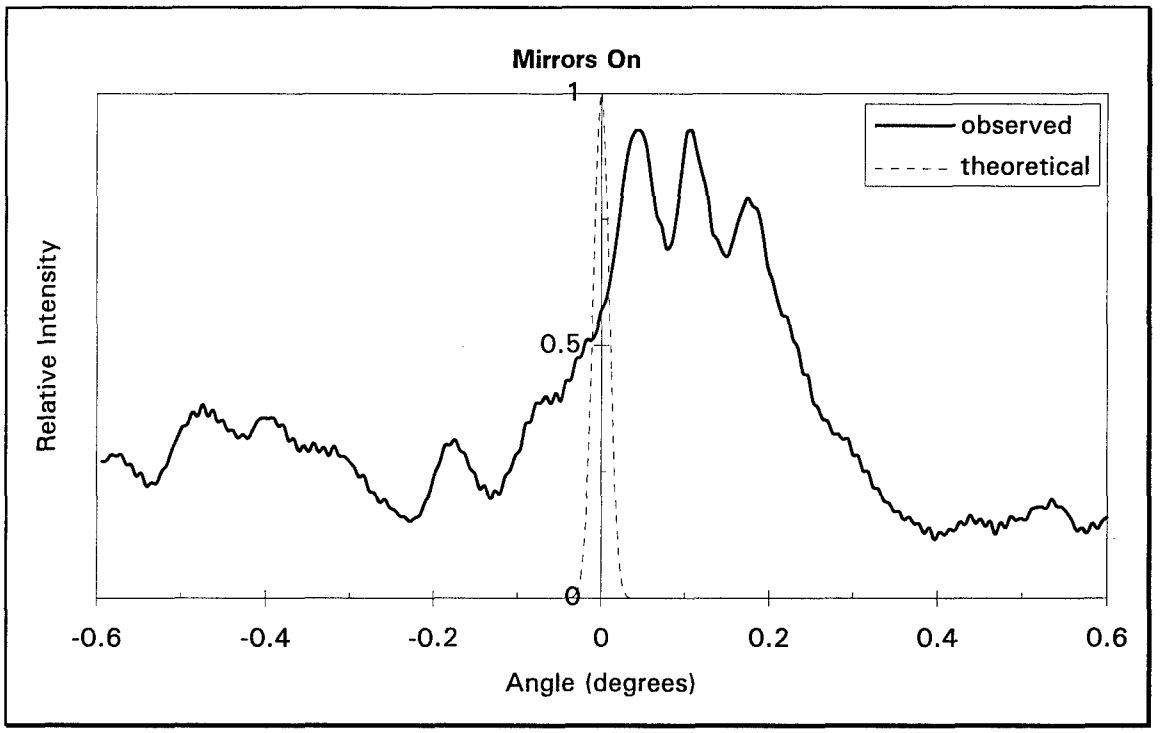

Figure 17c. Single Lobe in Far-Field (225 mA).

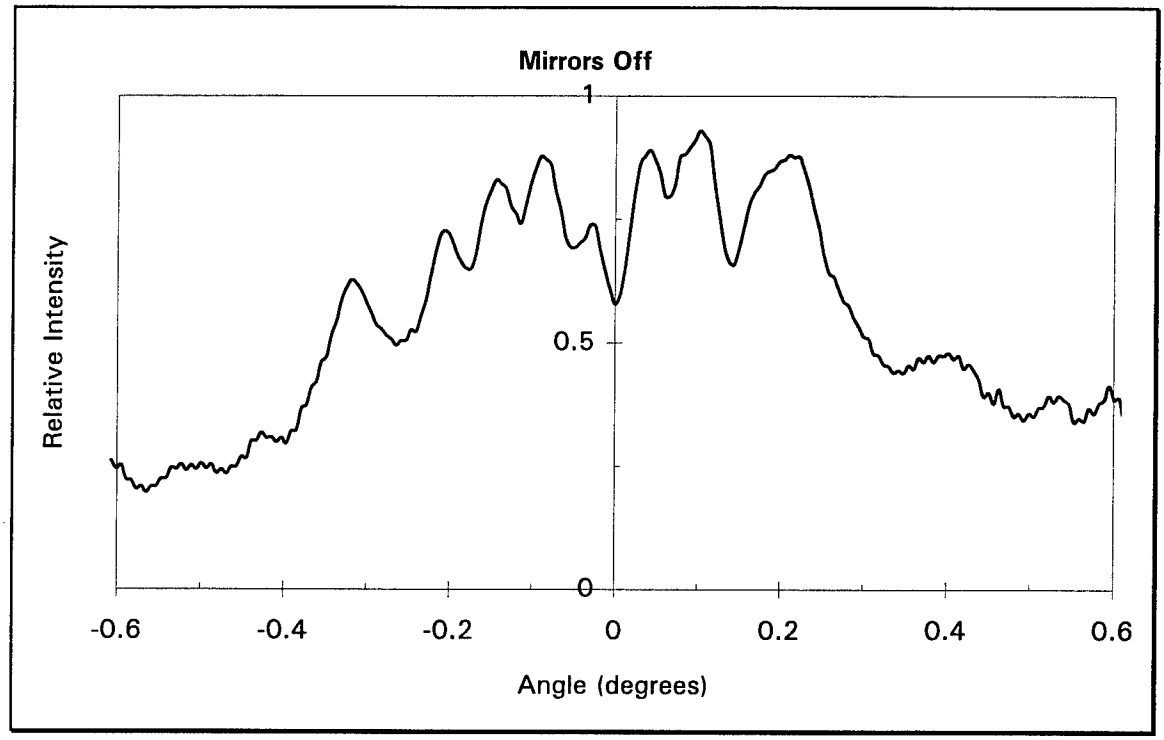

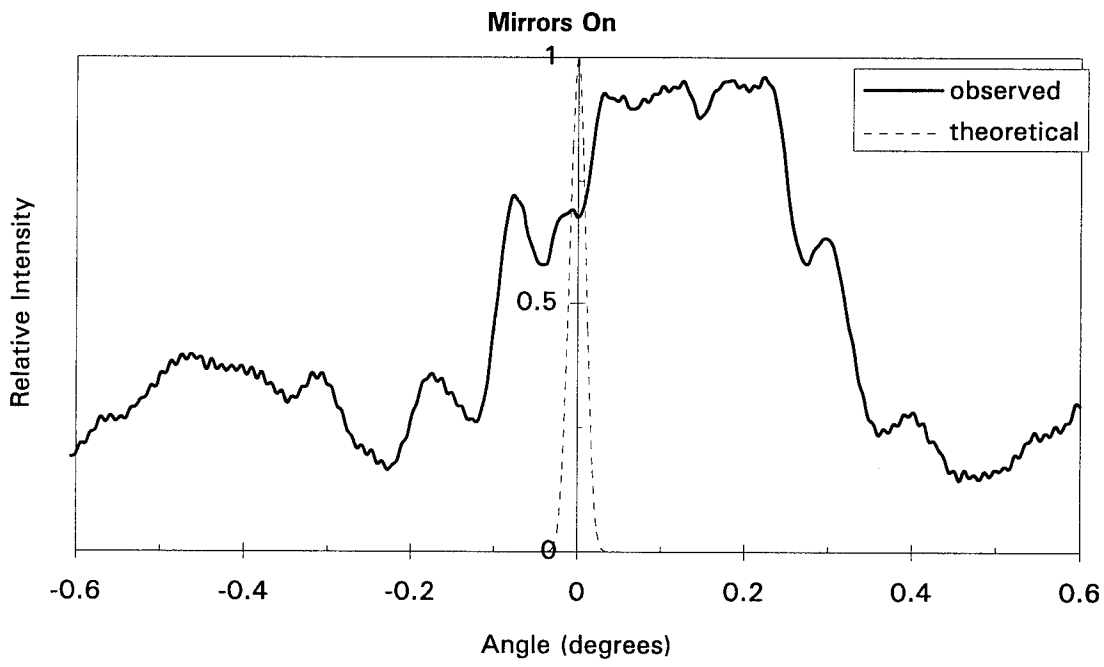

Figure 17d. Single Lobe in Far-Field (240 mA).

Phase Steering the Single Lobe

Next, the single lobe in the far-field was steered by adjusting the phasing of the LDA at the micromirror array. A table of the required phases for various steering angles was developed using Equation 3.11. Table 1 then gave the phasing required at each of the mirrors to produce the desired phase front. The mirror deflection required to produce this phasing was then calculated predicated on a wavelength of 828 nm:

$$deflection(nm) = \frac{\psi(828nm)}{4\pi} \tag{4.4}$$

The appropriate voltage for each mirror was then looked up from the mirror deflection charts. Table 7 lists only the voltages required for steering.

Appendix C shows the development of the phase steering equations. The appendix also contains a full chart showing the phasing, mirror deflections, and voltages required at each mirror for the various steering angles.

TABLE 7

Phase Steering Voltage Chart

MIRROR	$\theta = 0.1°$ Volts	$\theta = 0.2°$ Volts	$\theta = 0.3°$ Volts	$\theta = 0.4°$ Volts	$\theta = 0.475°$ Volts
M1	20.0	22	23.5	24.3	18.0
M2	18.3	15	12.3	8.0	20.5
M3	11.5	25.5	19.8	7.0	21.6
M4	16.1	24.7	11.2	22.4	26.3
M5	10.5/19.3	2.5/23.7	3.5	11.3	15.5
M6	0.0	0.0	0.0	0.0	0.0
M7	23.6/15.4	26.4/8.4	10.0	16.8	19.8
M8	18.4	25.6	14.0	23.5	27.2
M9	12.8	25.5	20.2	3.1	22.0
M10	24.5	22.5	18.5	15.5	26.5

M6 was suspected of being bad, therefore it was used as the center point of the steering pattern. It was always left at 0 V, no deflection. Equation 3.16 can be used to predict the maximum possible steering angles:

$$\psi = kb\ \mathrm{Sin}\theta \tag{3.16}$$

$$\theta_{MAX} = \mathrm{Sin}^{-1}(\lambda/b) \tag{4.5}$$

$\theta_{MAX} = \pm 0.475°$ with b = 100 μm. 100 μm is not the LDA element separation, it is the center - center separation of the mirrors. The phasing is changed at the mirrors, so it is the mirror spacing that determines the maximum steering angle.

In some cases, 2 voltages are listed in Table 7 for M5 and M7. These two mirrors control whether the beam is steered to the left or right. The first voltage listed is used to steer left and the second voltage will steer the beam to the right. When attempting to steer left or right to 0.3°, 0.4°, or 0.475°, the voltages were first set to the table values, then M5 and M7 were adjusted slightly depending upon the desired steering direction. For example, when steering to 0.3° left, M5 was set to 2 V and M7 to 20 V. To steer 0.3° right, M5 went to 10 V and M7 to 12 V. The pattern was thus determined. To steer left, M5 went lower than the chart and M7 went higher. To steer right, increase M5 deflection and decrease M7 deflection.

The steering tests were observed and measured using the same setup as in Figure 16, except for one change. The distance from the micromirrors to the Beamcode camera was increased from 267 mm to 360 mm. Table 8 lists the results of the beam steering tests. The tests were done at an injection current of 200 mA, therefore, the actual value in the

table is corrected for the + 0.065° offset experienced when obtaining a single lobe. In the table, minus is left, and plus is right.

TABLE 8

Steering Results

TARGET	ACTUAL	DELTA
-0.475	-0.480	-0.005
-0.40	-0.310	+0.090
-0.30	-0.270	+0.030
-0.20	-0.265	-0.065
-0.15	-0.154	-0.004
-0.10	-0.219	-0.109
+0.00	+0.00	+0.000
+0.10	+0.126	-0.026
+0.20	+0.182	-0.018
+0.30	+0.326	+0.026
+0.40	+0.185	-0.215
+0.475	+0.327	-0.148

The average steering error was ± 0.061°. In general the results were only fair. At first, the mirrors were set according to the chart values, and only adjusted to minimize sidelobes. The angle steered to was not determined until the next day when the data was analyzed. This resulted in the large errors reported for steering to: -0.40°, -0.10°, +0.40°.

Due to the large errors seen in the initial data, on subsequent days of data collection the method of steering was modified slightly. The target spot for steering was marked on the Beamcode monitor prior to steering. The mirrors would be set to the chart values and then driven as necessary to achieve the maximum laser power at the marked spot. At times, large sidelobes would appear in the intensity pattern as the main beam approached its target. Tradeoffs had to be made between hitting the target and minimizing sidelobes.

This accounts for the errors seen in Table 8 when steering to: -0.30°, -0.20°, and +0.10°. Steering in this manner sometimes required that the mirror voltages be set to a value that differed significantly from the predicted value. This can be seen in Table 9, which lists predicted and actual mirror voltages used for the steering.

Steering could be achieved, and the general direction of the beam predicted, but confidence in the accuracy was not very high. Steering was observed from 0.480° left to 0.327° right, a range of 0.807°. The predicted range was 0.95°.

The graphs that follow are illustrations of the steering results. Figure 18a shows the beam steered to +0.1°, the center of the peak is at a corrected value of 0.126°. In Figure 18b, the lobe is steered to -.15°, and 18c represents steering to -0.475°. Figure 18d shows what would be a good steering pattern to +0.20°, but multiple sidelobes are present, and Figure 18e represents maximum achievable steering to the right. The peak is at +0.327° and could not be driven any farther.

TABLE 9						
Mirror Voltage Steering Chart						
Angle =		0.1	-0.1		0.2	-0.2
	Predicted	Actual	Actual	Predicted	Actual	Actual
	Volts	Volts	Volts	Volts	Volts	Volts
M1	20.0	19.0	16.0	22.0	12.5	22.0
M2	18.3	18.0	22.0	15.0	24.0	14.0
M3	11.5	24.0	14.0	25.5	25.0	26.0
M4	16.1	15.0	19.0	24.7	19.0	24.0
M5	10.5/19.3	19.0	5.0	2.5/23.7	7.0	19.0
M6	0.0	0.0	0.0	0.0	0.0	0.0
M7	23.6/15.4	15.0	27.0	26.4/8.4	28.0	11.0
M8	18.4	18.0	16.0	25.6	15.0	26.0
M9	12.8	17.0	9.0	25.5	17.0	26.0
M10	24.5	24.0	22.0	22.5	19.0	22.0
Angle =		0.3	-0.3		0.4	-0.4
	Predicted	Actual	Actual	Predicted	Actual	Actual
	Volts	Volts	Volts	Volts	Volts	Volts
M1	23.5	18.0	17.0	24.3	14.0	22.0
M2	12.3	12.0	13.0	8.0	7.0	8.0
M3	19.8	21.0	22.0	7.0	0.0	7.0
M4	11.2	11.0	13.0	22.4	20.0	22.0
M5	3.5	10.0	2.0	11.3	17.0	23.0
M6	0.0	0.0	0.0	0.0	0.0	0.0
M7	10.0	12.0	20.0	16.8	18.0	15.0
M8	14.0	21.0	23.0	23.5	22.0	24.0
M9	20.2	17.0	14.0	3.1	4.0	5.0
M10	18.5	19.0	16.0	15.5	15.0	16.0
Angle =		0.475	-0.475			
	Predicted	Actual	Actual			
	Volts	Volts	Volts			
M1	18.0	15.0	16.0			
M2	20.5	26.0	17.0			
M3	21.6	20.0	18.0			
M4	26.3	26.0	21.0			
M5	15.5	28.0	19.0			
M6	0.0	0.0	0.0			
M7	19.8	26.0	22.0			
M8	27.2	24.0	23.0			
M9	22.0	25.0	22.0			
M10	26.5	22.0	24.0			

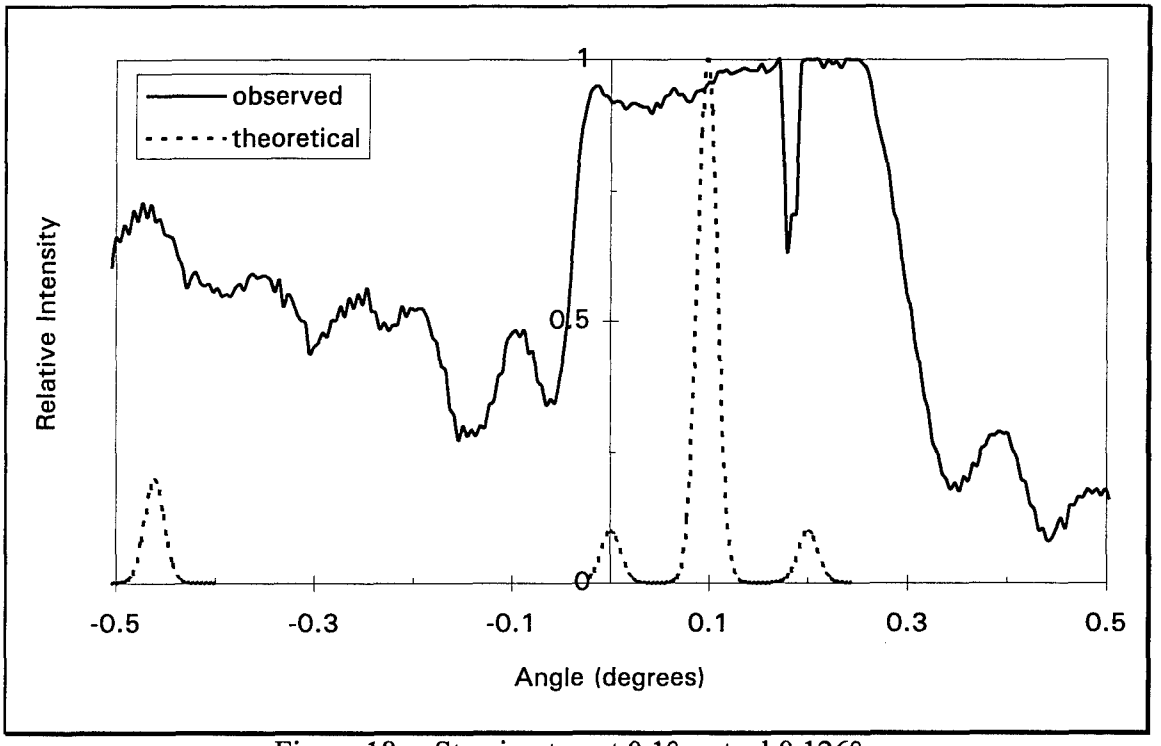

Figure 18a. Steering target 0.1°, actual 0.126°.

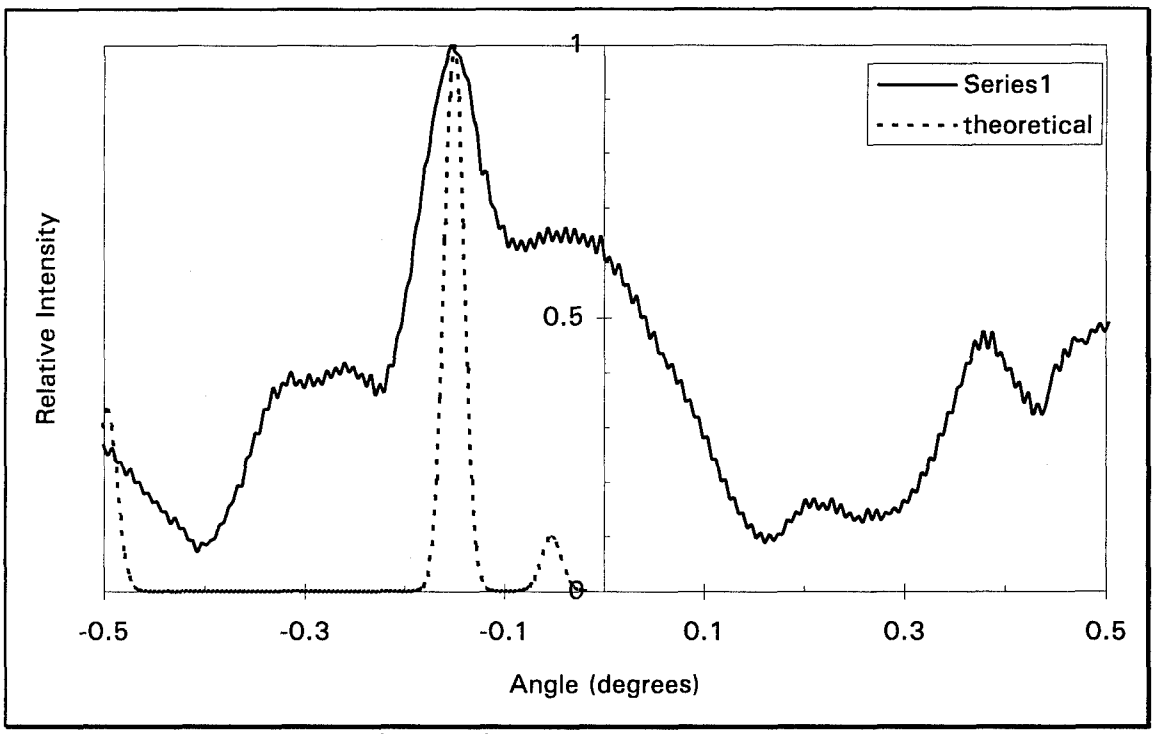

Figure 18b. Steering target -0.15°, actual -0.154°.

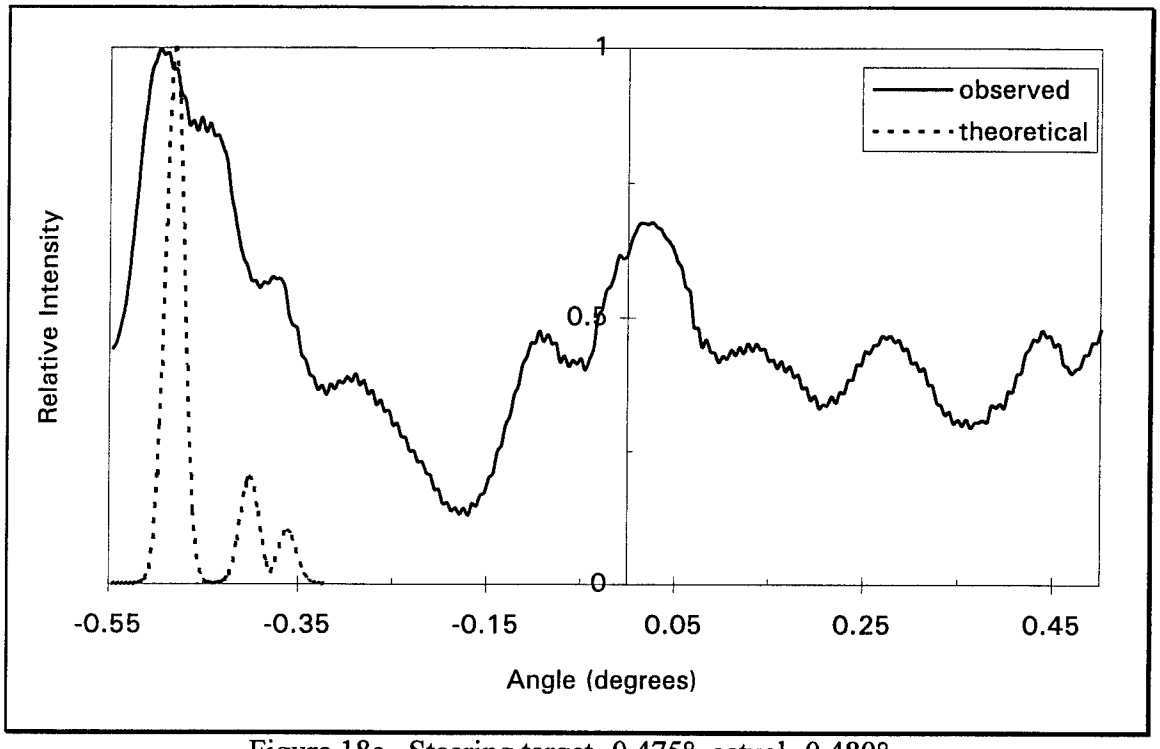

Figure 18c. Steering target -0.475°, actual -0.480°.

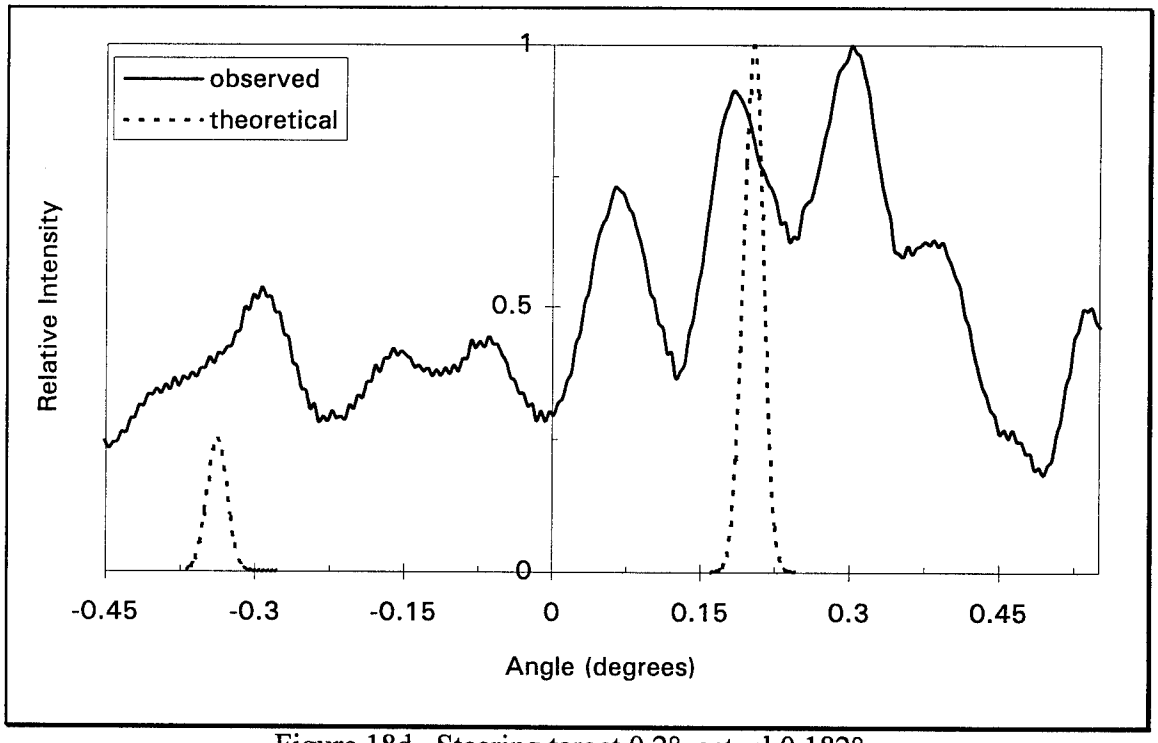

Figure 18d. Steering target 0.2°, actual 0.182°.

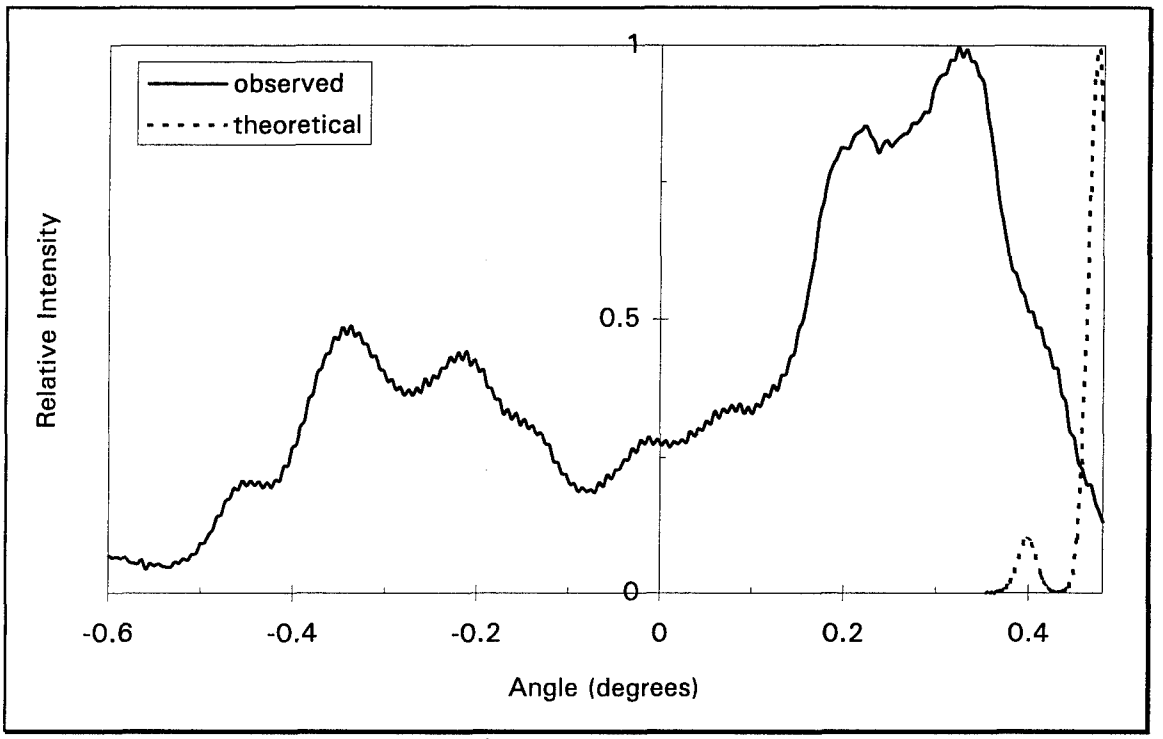

Figure 18e. Steering target 0.475°, actual 0.327°.

V. Conclusions and Recommendations

Conclusions

A novel and practical technique to control and direct the output of a laser diode array (LDA) was investigated and demonstrated. A ten element micromirror array was developed, tested, and employed to produce a single spot in the far-field of a ten element LDA operating in the fundamental out-of-phase supermode. The micromirror array was also utilized to phase steer the single spot.

Before the laser output could be manipulated, the LDA had to be characterized. The operating parameters of the LDA were studied to aid the researcher's understanding of how laser diodes perform. Two of the measurements were critical to the success of the project. They were emission spectra, and measurement of the phase difference between adjacent elements.

Emission spectra was observed to measure the wavelength of the LDA. The wavelength was determined to be centered around 828.38 nm with peaks of the multiple longitudinal modes occurring from 827.46 to 828.89 nm. This data was used to determine the initial settings of the mirrors to phase shift the LDA output.

The phase difference ($\Delta\phi$) between adjacent elements was observed using two slit diffraction. This confirmed that $\Delta\phi$ was 180°, and that to obtain a single spot every other element of the LDA needed to be phase shifted by this amount.

The micromirror array also required characterization before use. The amount of deflection a D. C. voltage would produce was measured. It was noted that the deflection response to voltage was more exponential than linear. Also the response varied from mirror to mirror so that each mirror had to have its own calibration chart. And finally, that applying a voltage to one mirror would cause other mirrors to move. Crosstalk could be counteracted by grounding mirrors to prevent unwanted movement.

Once the LDA and micromirror array were understood, they were used together to obtain a single lobe in the far-field. This portion of the experiment had great success. A strong single lobe was obtained for several different injection currents. The single lobe was narrower than the uncontrolled far-field lobes. A spot with a FWHM as narrow as 0.167° was observed.

It was also observed that when adjusting the mirrors, lines of intensity could be seen moving across the screen. This suggests that a LDA operating in any supermode can be adjusted to all in-phase operation by adjusting the mirrors while observing the LDA output. Prior knowledge of the phase relationships, while helpful, would not be essential to success.

Next, the single lobe was steered. Steering was achieved, however, the complex interaction of the LDA phases made exact predictions of the steering angles difficult. Sidelobes also made steering to some angles even more difficult. In spite of these problems, steering to 12 separate spots over a 0.807° range was demonstrated.

This demonstration proved the feasibility of using a micromirror array to control the LDA. The method has many advantages over more elaborate schemes. The device is inexpensive and compact. It is elegant in its simplicity, versatility, and reliability.

Recommendations

Since the concept has been proven, the potential exists for application to a variety of military and commercial uses. Several of the uses mentioned in the introduction could benefit from the employment of such a device.

Further study of micromirror arrays is also warranted. Three design improvements for future possible designs come to mind. First, make the mirrors as large as possible without changing the center to center spacing. At 100 μm spacing, mirrors with a 90 μm diameter are possible. Also, the etch hole in the center of the mirrors should be omitted from the design. The metal plating should be applied only on the mirrors, not on the entire array structure. The combination of these improvements would improve reflectivity, allow operation at higher currents, and reduce light lost to scatter.

To improve steering reliability, a chart could be constructed giving the best mirror voltages for all desired steering angles. Time constraints prevented the construction of such a chart during this study.

Finally, methods of reducing sidelobes should be explored. Methods may exist to optimize the steering with control of phase only.[39]

Appendix A: The Micromirror Array

Physically, the micromirror array is a set of ten mirrors placed side by side on a single structure. Each mirror is attached to the structure via mounting flexures. The mirrors are hexagonal in shape and are 60 μm across. The center to center spacing of the mirrors is 100 μm. Figure 19a is a CAD drawing of the array. Figure 19b is a SEM photograph of the array, and Figure 19c shows details of an individual mirror. The dimensions chosen for the array are exactly 10 × the dimensions of the elements of the LDA to be used for testing.

The micromirror array is mounted on a semiconductor chip and each mirror can be moved independently. When a voltage is applied between a mirror and its address electrode, the electrostatic force pulls the mirror downward towards the address electrode. This downward pull is countered by the upward spring force of the mirror mounting flexures.[40] Therefore, an applied DC voltage produces a static deflection of the mirror.

These mirrors were invented by Larry Hornbeck of Texas Instruments approximately 15 years ago. Two dimensional arrays of micromirrors are currently being used to produce high resolution video displays.[41]

The array used in this project was constructed using standard semiconductor manufacturing techniques. The array was designed by students in the Electrical Engineering Department at the Air Force Institute of Technology (AFIT) using Cadence software. The device was then fabricated by Microelectronics Corporation of North

Carolina (MCNC), in their Micro-Electro-Mechanical Systems (MEMS) Technology Applications Center.

The process begins with a silicon wafer that is doped with $POCl_3$. A 605 nm silicon nitride layer is applied to the wafer for electrical isolation. Over this a 488 nm layer of polysilicon film (Poly 0) is applied. The Poly 0 is lithographically etched to form the address electrodes of the array. Then a sacrificial layer of photosilicate glass (PSG), a 1470.6 nm layer of polysilicon film (Poly 2), and another layer of PSG are applied. The wafer is then annealed for one hour at 1050° C to dope and crystallize the Poly 2 layer. The Poly 2 and the layer of PSG above it are then etched to form the mirrors and flexures. A 531.8 nm layer of Chromium/Gold alloy is deposited over the Poly 2 to increase the reflectivity of the surface. When a sacrificial release of the lower PSG layer is performed, 2040 nm of free space is created between the Poly 2 layer and the Poly 0 layer, except at the anchor points. Anchor points are located at each end of the mirror array in the Poly 2 layer to hold the array in place.[42] The mirrors are now suspended above their address electrodes by their flexures and will move when a voltage is applied.

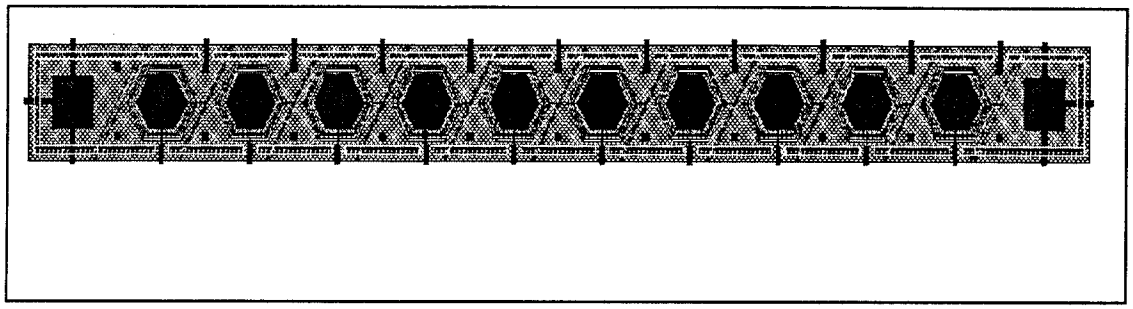

Figure 19a. CAD Drawing of Miromirror Array.

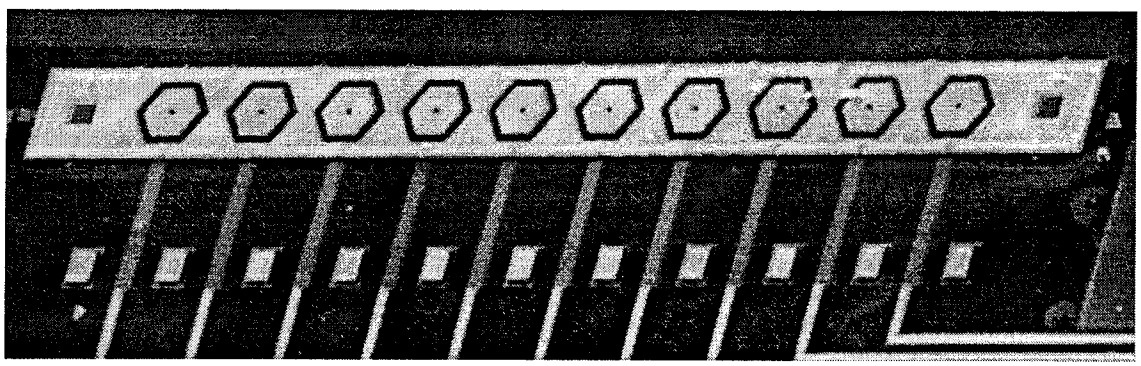

Figure 19b. Microscope Photograph of the Miromirror Array.

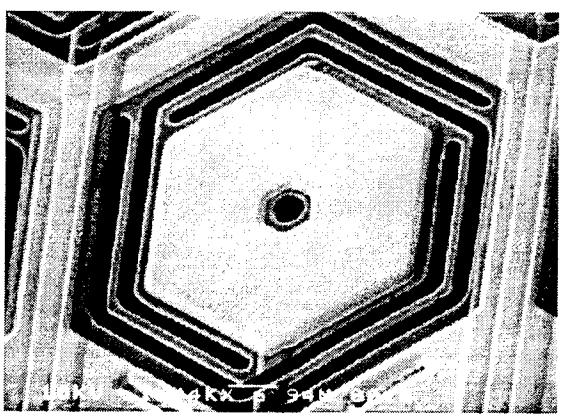

Figure 19c. Photograph of a Single Mirror to Show Detail.

Appendix B: Numerical Approximation of the Far-Field Intensity Pattern of the LDA

The far-field intensity pattern can be predicted using numerical methods. A line scan of the near-field intensity pattern is read into Mathematica as an array. To approximate the electric field distribution of the LDA, the square root of each element is taken and then every other peak is inverted to simulate the phase difference between elements. Sufficient 0's are added to the array so that the number of elements in the array is 2^n. Figure 20 shows a plot of the array. The similarity to Figure 10b, the near-field intensity pattern, is readily apparent.

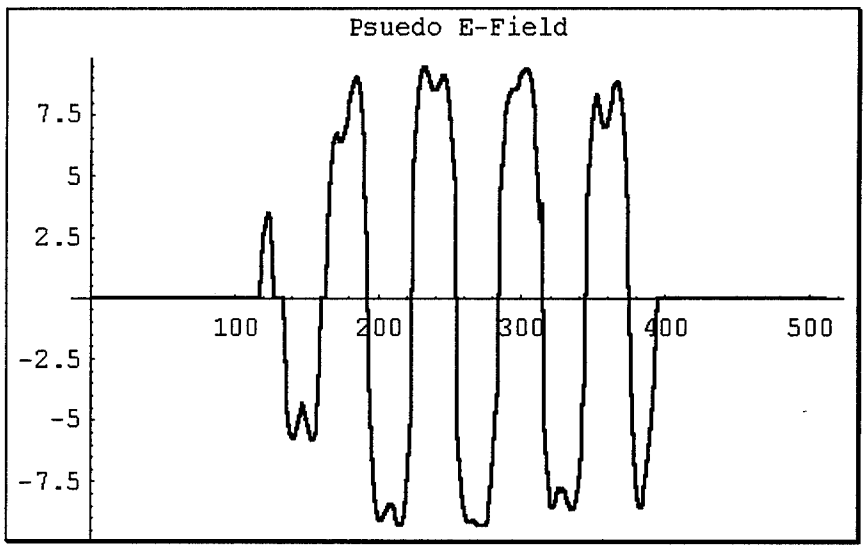

Figure 20. Simulation of Electric Field.

Using the assumption that the center to center spacing of the peaks in Figure 20 is

10 μm, an analysis of the figure determines that dx, the size of each element of the array, = 0.333 nm.

The far-field electric field is determined by taking the Fourier transform of the near-field. A Fourier transform of the array can be performed numerically with Mathematica.

nf=RotateLeft[near, 256]//N (B.1)

fort=Fourier[nf]//N (B.2)

ft=RotateRight[fort,256]//N (B.3)

The electric field cannot be measured, but the intensity can. The intensity pattern is the modulus squared of the Fourier transform. This yields the numerical model of the far-field intensity pattern shown in Figure 21.

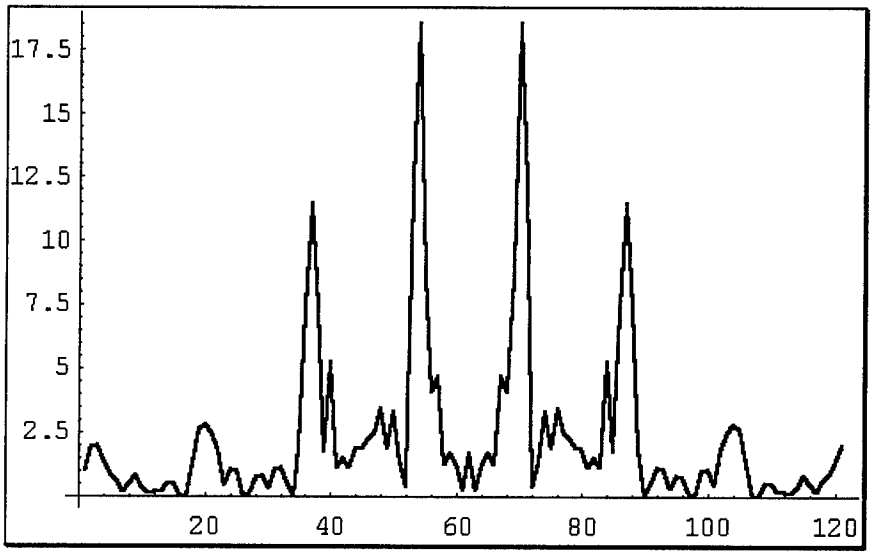

Figure 21. Numerical Model of the Far-Field Intensity Pattern

The Fourier transform takes the function from the spatial regime to the frequency domain. The "x axis" in Figure 21 is now in units of θ, where $f = \theta/\lambda$. To determine the sample size of the graph, the following relationship is used:

$$\partial f = \frac{\partial\theta}{\lambda} = \frac{1}{N\partial x} = 5859.375 \tag{B.4}$$

where N = 512, the number of elements in the array, and λ = 828 nm. Therefore:

$$\partial\theta = \partial f \cdot \lambda = 4.857 \cdot 10^{-3} \frac{rad}{sample} \tag{B.5}$$

The two dominant peaks in Figure 21 represent the two lobes of the far-field intensity pattern. Measurement of the peaks' displacement from the center of the pattern show that the left lobe is at $6 \cdot d\theta = 0.029$ rads. The right peak is $10 \cdot d\theta = 0.049$ rads.

Figure 21 therefore predicts that the far-field intensity pattern will have two main peaks about the center of the pattern. They will be much stronger in amplitude than the near-field intensity peaks, and spaced 0.078 = 4.45° apart. This is in close agreement with the analytic prediction (4.53°) and also compares favorably with the actually measured far-field intensity.

Appendix C: Phase Steering Equations

The amount of element to element phase required for steering was given in Equation 3.16:

$$\psi = kb\ \mathrm{Sin}(\theta) \tag{3.16}$$

where $k = 2\pi/\lambda = 757.923\ nm^{-1}$. The maximum possible steering angle was determined in Chapter 3 to be 0.475°. Table 10 shows the element to element phase required for steering in steps of $\theta = 0.1°$.

TABLE 10

Phase Steering

Steer Angle θ (degrees)	ψ (radians)	ψ (degrees)
0.0	0.0	0.0
0.1	1.32283	75.7923
0.2	2.64565	151.584
0.3	3.96846	227.376
0.4	5.29126	303.167
0.475	6.28319	360.000

The phasing for each mirror of the array is found using Table 1 in Chapter 3.

TABLE 1

Mirror Phases for Beam Steering

Mirror	Phase	Mirror	Phase
1	$\pi - 5\psi$	6	0
2	-4ψ	7	$\pi + \psi$
3	$\pi - 3\psi$	8	2ψ
4	-2ψ	9	$\pi + 3\psi$
5	$\pi - \psi$	10	4ψ

The required phase at each mirror is normalized to 360° as necessary. Then mirror deflection is given by Equation 4.4:

$$deflection(nm) = \frac{\psi(828nm)}{4\pi} \tag{4.4}$$

The required voltage is obtained from the mirror calibration charts, resulting in:

TABLE 11

Phase Steering

	θ = 0.1°			θ = 0.2°			θ = 0.3°		
	PHASE deg.	DEF. nm	VOLTS	PHASE deg	DEF. nm	VOLTS	PHASE deg	DEF. nm	VOLTS
M1	199	229	20	217	251	22.0	237	272	23.5
M2	303	349	18.2	246	283	15.0	189	218	12.3
M3	47	54	11.5	275	316	25.5	142	163	19.8
M4	152	174	16.1	303	349	24.7	95	109	11.2
M5	104	120	10.5	28	33	2.5	47	54	3.5
M7	256	294	23.6	332	381	26.4	47	54	10.0
M8	152	174	18.4	303	349	25.6	95	109	14.0
M9	47	54	12.8	275	316	25.5	142	163	20.2
M10	303	349	24.5	246	283	22.5	189	218	18.5
	θ = 0.4°			θ = 0.47 5°					
	PHASE deg	DEF. nm	VOLTS	PHASE deg	DEF. nm	VOLTS			
M1	256	294	24.3	179	206	26.5			
M2	133	153	8	359	413	18.0			
M3	9	11	7	179	206	20.5			
M4	246	283	22.4	359	413	21.6			
M5	123	142	11.3	180	207	26.3			
M7	123	142	16.8	180	207	15.5			
M8	246	283	23.5	359	413	19.8			
M9	9	11	3.1	179	206	27.3			
M10	133	153	15.5	359	413	26.5			

These voltages are the same ones given in Table 7.

BIBLIOGRAPHY

1. Grossman, Jonathan G. Military Laser Systems, Rand Report, Rand Corporation, Rand P-7704 (1991).

2. Schwartz, William. "Solid-state lasers point to the future in military applications," Laser Focus World, 27 (7): 75-96 (July 1991).

3. Higgins, Thomas V. "The smaller, cheaper, faster world of the laser diode," Laser Focus World, 31 (4): 66-73 (April 1995).

4. Spectra Diode Labs. Laser Diode Operator's Manual. San Jose, CA. (October 1991).

5. Striefer, W., R. D. Burnham, T. L. Paoli, and R. D. Scifres. "Phased array diode lasers," Laser Focus/Electro-Optics, 20 (6): 100-108 (June 1984).

6. Matsumoto, M., M. Taneya, S. Matsui, S. Yano, and T. Hijikata. "Single-lobed far-field pattern operation in a phased array with an integrated phase shifter," Applied Physics Letters, 50 (22): 1541-1543 (June 1987).

7. Botez, Dan and R. Scifres. Diode Laser Arrays. New York, NY. Cambridge University Press, 1994.

8. Hecht, Eugene. Optics. Reading, MA. Addison-Wesley Publishing, 1987.

9. Verdeyen, Joseph T. Laser Electronics. Englewood Cliffs, NJ. Prentice Hall, 1995.

10. Summers, Thomas A. Generation of a Single-Lobe, Far Field Intensity Pattern From a Laser Diode Array Using an Optical Delay Line. MS Thesis, AFIT/GAP/ENP/94D-10. School of Engineering, Air Force Institute of Technology (AU), Wright Patterson AFB, OH, December 1994.

11. Thompson, G. H. B. Physics of Semiconductor Laser Devices. New York, NY. John Wiley & Sons, 1980.

12. Tatsuno, Kimio, et al. "Diffraction-limited circular single spot from phased array lasers," Applied Optics, 28 (21): 4650-4657 (1 November 1989).

13. Waarts, Robert, et al. "High power, CW, diffraction-limited, GaAlAs laser diode array in an external Talbot cavity," Applied Physics Letters, 58 (23): 2586-2588 (June 1991).

14. Leger, James R., M. L. Scott, and W. B. Veldkamp. "Coherent addition of AlGaAs lasers using microlenses and diffractive coupling," Applied Physics Letters, 52 (21): 1771-1773 (May 1988).

15. Chang-Hasnain, C. et al. "Diffraction-limited emission from a diode laser array in an aperture graded index lens external cavity," Applied Physics Letters, 49 (11): 614-616 (September 1986).

16. Segev, Mordechai, and Baruch Fischer. "Laser diode arrays with apertured phase conjugate feedback," Quantum Electronics Letters, 26 (8): 1318-1322 (August 1990).

17. Jackson, G. S., N. Holonyak Jr., and D. C. Hall. "Supermode behavior of coupled two-stripe $Al_xGa_{1-x}As$-GaAs quantum well heterostructure lasers," Journal of Applied Physics, 62 (2): 381-385 (15 July 1987).

18. Beernik, K. J., J. J. Alwan, and J. J. Coleman. "InGaAS-GaAs-AlGaAs gain-guided arrays operating in the in-phase fundamental array mode," Applied Physics Letters, 57 (26): 2764-2766 (24 December 1990).

19. Hohimer, J. P., A. Owyoung, and G. R. Hadley. "Single channel injection locking of a diode laser array with a cw dye laser," Applied Physics Letters, 47 (12): 1244-1246 (December 1985).

20. Hadley, G. Ronald, A. Owyoung, and J. P. Hohimer. "Modeling of injection locking phenomena in diode laser arrays," Optics Letters, 11 (3): 144-146 (March 1986).

21. Chun, Myung K., T. L. Whitman, and D. G. Soenksen. "Far-field behavior of injection locked semiconductor laser arrays," Applied Optics, 26 (21): 4518-4521 (November 1987).

22. MacCormack, Stuart, and Robert W. Eason. "Near-diffraction-limited single-lobe emission from a high-power diode-laser array coupled to a photorefractive self-pumped phase-conjugate mirror," Optics Letters, 16 (10): 705-707 (15 May 1991).

23. Taneya, M., M. Matsumoto, S. Yano, and T. Hijikata. "Stable quasi 0° mode operation in a laser diode array nearly aligned with a phase shifter," Applied Physics Letters, 50 (13): 783-785 (30 March 1987).

24. Matsumoto, M., M. Taneya, S. Yano, and T. Hijikata. "Single-lobed far-field pattern operation in a phased array with an integrated phase shifter," Applied Physics Letters, 50 (22): 1541-1543 (1 June 1987).

25. Thaniyavarn, S., and W. Dougherty. "Generation of a single lobe radiation pattern from a phased array laser using a near-contact variable phase shift zone plate," Electronics Letters, 23 (1): 5-7 (2 January 1987).

26. Goltsos, William, and Michael Holz. "Agile beam steering using binary optics microlens arrays," Optical Engineering, 29 (11): 1392-1397 (November 1990).

27. Motamedi, M. Edward, A. P. Andrews, W. J. Gunning, and M. Khoshnevisan. "Miniaturized micro-optical scanners," Optical Engineering, 33 (11): 3616-3623 (November 1994).

28. Farn, Michael W. "Agile beam steering using phased-arraylike binary optics," Applied Optics, 33 (22): 5151-5158 (1 August 1994).

29. Sun, Y., D. A. Francis, S. A. Biellak, A. E. Siegman, and C. J. Chang-Hasnain. "Beam steerable semiconductor lasers with large steering range and resolvable spots," Electronics Letters, 30 (24): 2034-2035 (24 November 1994).

30. Kenyon, Gregory S. Characterization of an LCD For Use as a Programmable Phase Shifter to Produce a Single Lobed Far-Field Pattern in a Phased Array. MS thesis, AFIT/GAP/ENP/93D-05. School of Engineering, Air Force Institute of Technology (AU), Wright Patterson AFB, OH, December 1993.

31. Zhou, Shaomin, P. Yeh, and H. Liu. "Dynamic two-dimensional beam-pattern steering technique," Optics Letters, 18 (11): 843-845 (1 June 1993).

32. McManamon, Paul F., E. A. Watson, T. A. Dorschner, and L. J. Barnes. "Nonmechanical beam steering for active and passive sensors," SPIE, 1969: 2-10 (August 1993).

33. Butler, J. K., D. E. Ackley, and D. Botez. "Coupled mode analysis of phased-locked injection laser arrays," Applied Physics Letters, 44 (3): 293-295 (1 February 1984).

34. Botez, Dan. "Array mode far-field patterns for phase-locked diode laser arrays: Coupled mode theory versus simple diffraction theory," IEEE Journal of Quantum Electronics, QE-21 (11): 1752-1755 (11 November 1985).

35. Saleh, Bahaa E. A., and Malvin Carl Teich. Fundamentals of Photonics. New York, NY. John Wiley & Sons, 1991.

36. Goodman, Joseph W. Introduction to Fourier Optics. San Francisco, CA. McGraw-Hill Inc., 1968.

37. Carlson, N. W., V. J. Masin, M. Lurie, B. Goldstein, and G. A. Evans. "Measurement of the coherence of a single-mode phase-locked diode laser array," Applied Physics Letters, 51 (9): 643-645 (31 August 1987).

38. Oliner, Arthur A., and George H. Knittel. Phased Array Antennas. Dedham, MA. Artech House, Inc., 1972.

39. DeFord, John F., and Om P. Ghandi. "Phase-Only Synthesis of Minimum Peak Sidelobe Patterns for Linear and Planar Arrays," IEEE Transactions on Antennas and Propagation, 36 (2): 191-201 (February 1988).

40. Michalicek, M. Adrian. Design, Fabrication, Modeling, and Testing of Surface-Micromachined Micromirror Devices. MS Thesis, AFIT/GE/ENG/95J-01. School of Engineering, Air Force Institute of Technology (AU), Wright Patterson AFB, OH, 1 June 1995.

41. Younse, Jack M. "Mirrors on a chip," IEEE Spectrum, 30 (11): 27-31 (November 1993).

42. Koester, David A., et al. "Multi-user MEMS process introduction and design rules," MCNC, MEMS Technology Applications Center, Research Triangle Park, North Carolina (October 1994).

Vita

Captain Carl J. Christensen [redacted] California. He spent his early years in Northern California, graduating from Jesuit High School in Sacramento, California in June, 1975. He entered the Air Force in 1978 and worked as an avionics technician for 12 years. After graduating from Minot State University with a Bachelor of Arts degree in Physics in 1989, he attended Officer Training School, receiving a reserve commission in October 1990. His first assignment after OTS was to 3 SOPS, Falcon AFB, Colorado where he served as a Ground Control Officer, NATO III Crew Commander, and Flight Commander. In May, 1994 he entered the School of Engineering, Air Force Institute of Technology where he will graduate in December, 1995 with a Master of Science in Engineering Physics. His follow-on assignment is to the Air Force Technical Applications Center (AFTAC), McClellan AFB, California.

[redacted]

REPORT DOCUMENTATION PAGE

Form Approved
OMB No. 0704-0188

1. AGENCY USE ONLY *(Leave blank)*	2. REPORT DATE	3. REPORT TYPE AND DATES COVERED
	DEC 95	

4. TITLE AND SUBTITLE
MICROMIRROR ARRAY CONTROL OF A PHASE-LOCKED LASER DIODE ARRAY

5. FUNDING NUMBERS

6. AUTHOR(S)
Christensen Carl J.

7. PERFORMING ORGANIZATION NAME(S) AND ADDRESS(ES)
AFIT/ENP
2950 P Street
Wright Patterson AFB, OH 45433
(Capt Jeff Grantham)

8. PERFORMING ORGANIZATION REPORT NUMBER
AFIT/GAP/ENP/95D-2

9. SPONSORING/MONITORING AGENCY NAME(S) AND ADDRESS(ES)
N/A

10. SPONSORING/MONITORING AGENCY REPORT NUMBER

11. SUPPLEMENTARY NOTES

12a. DISTRIBUTION/AVAILABILITY STATEMENT
Approved for public release; distribution unlimited

12b. DISTRIBUTION CODE

13. ABSTRACT *(Maximum 200 words)*

A ten element micromirror array has been designed, fabricated, and employed to cintrol the far-field irradiance pattern of a phased locked laser diode array. The laser used in this experiment was a ten element laser array operating in the pi out-of-phase supermode. The laser near-field irradiance was imaged onto the micromirrot array, where the phasing was adjusted so all the elements were in-phase, producing the desirable single lobe far-field pattern. The micro mirror array was also used to phase steer the reflected laser beam. In analogy to phased array radar steering, a small phase difference was introduced between adjacent elements of the array. The phase front introduced across the array steered the single lobe across a 0.807 degree range.

14. SUBJECT TERMS
Micromirror
MEMS
Laser Diode Array
Far-field
Phase Steering
Supermodes

15. NUMBER OF PAGES
83

16. PRICE CODE

17. SECURITY CLASSIFICATION OF REPORT	18. SECURITY CLASSIFICATION OF THIS PAGE	19. SECURITY CLASSIFICATION OF ABSTRACT	20. LIMITATION OF ABSTRACT